CONTENTS

Report Documentation Page

Form Approved
OMB No. 0704-0188

1. REPORT DATE	2. REPORT TYPE	3. DATES COVERED
06 JUN 2011		

4. TITLE AND SUBTITLE	5a. CONTRACT NUMBER
Examination and Manipulation of Clay Aggregates - Initial Inquiry	5b. GRANT NUMBER
	5c. PROGRAM ELEMENT NUMBER
6. AUTHOR(S)	5d. PROJECT NUMBER
Andrei Abelev	5e. TASK NUMBER
	5f. WORK UNIT NUMBER
7. PERFORMING ORGANIZATION NAME(S) AND ADDRESS(ES)	8. PERFORMING ORGANIZATION REPORT NUMBER
Naval Research Laboratory,4555 Overlook Avenue SW,Washington,DC,20375-5320	**NRL/FR/7420--11-10206**
9. SPONSORING/MONITORING AGENCY NAME(S) AND ADDRESS(ES)	10. SPONSOR/MONITOR'S ACRONYM(S)
	11. SPONSOR/MONITOR'S REPORT NUMBER(S)

12. DISTRIBUTION/AVAILABILITY STATEMENT

Approved for public release; distribution unlimited.

13. SUPPLEMENTARY NOTES

The original document contains color images.

14. ABSTRACT

This report discusses an initial experimental effort and the first conclusions in the examination and testing of clay aggregates composed of montmorillonite clay and a polysaccharide (xanthan gum, also called X-gum) in water of variable salinity undertaken at the Oakland University biolab in collaboration with K. Lesich.

15. SUBJECT TERMS

16. SECURITY CLASSIFICATION OF:			17. LIMITATION OF ABSTRACT	18. NUMBER OF PAGES	19a. NAME OF RESPONSIBLE PERSON
a. REPORT	b. ABSTRACT	c. THIS PAGE			
unclassified	**unclassified**	**unclassified**		**35**	

EXAMINATION AND MANIPULATION OF CLAY AGGREGATES – INITIAL INQUIRY

1. INTRODUCTION

This report discusses an initial experimental effort and the first conclusions in the examination and testing of clay aggregates composed of montmorillonite clay and a polysaccharide (xanthan gum, also called X-gum) in water of variable salinity undertaken at the Oakland University biolab in collaboration with K. Lesich.

The agenda for this work was as follows:

1. Floc size and morphology analysis
    - aggregation as a function of salinity
    - aggregation as a function of X-gum : clay ratio
2. Micro-pipettes preparation
    - drawing
    - bending
    - force-displacement calibration
3. Floc manipulation and testing
4. Conclusions, with implication on equipment and procedures for NRL floc testing

Overall, the work conducted may be classified as successful. A large number of lessons have been learned. This experience is highly relevant to the successful implementation of the NRL testing system and procedures for floc force testing. Several aspects of this preliminary experiment could not be completed in part due to the particular equipment configuration at Oakland University as not best suited for the types of tests we needed to conduct. Some improvised solutions were found, however, and important conclusions were reached on how best to improve and adapt this configuration.

2. FLOC SIZE AND MORPHOLOGY ANALYSIS

This section describes the results of the visual observation of the aggregates, prepared by A. Reed and J. Dale. The summary of the suspensions is given in Table 1, with salinity varying from 0 to 35 PSU and the X-gum content from 0% to 10% of the mineral content of the clay (by weight). Montmorillonite was used in all the suspensions prepared. This report discusses individual samples and draws initial conclusions about the apparent floc structure and dependence on the variables (X-gum, salinity), based only on the morphological analysis. Additionally, for each image of the floc presented, the type of optics and magnification used are noted. The set of objectives examined were the PLAN APO and PLAN FLUOR objectives by Nikon, with magnifications of 10X, 20X, and 40X.

Manuscript approved May 24, 2011.

Table 1 –Flocculation Sample List (A. Reed, J. Dale)

Sample No.	Montmorillonite	Salinity (PSU)	Xanthan Gum (% of Clay)
1	1 mg/mL	0	0
2	″	5	0
3	″	10	0
4	″	15	0
5	″	20	0
6	″	25	0
7	″	30	0
8	″	35	0
9	″	0	5
10	″	5	5
11	″	10	5
12	″	15	5
13	″	20	5
14	″	25	5
15	″	30	5
16	″	35	5
17	″	0	10
18	″	5	10
19	″	10	10
20	″	15	10
21	″	20	10
22	″	25	10
23	″	30	10
24	″	35	10

First, the visual evidence is presented – a variety of flocs from several selected samples. All specimens were imaged using a Nikon T2000U system and objectives with high numerical aperture values (NA), demonstrating a good quality optics set. The specimens were imaged in the custom-made imaging chambers that consisted of a cut-out plexiglas sheet (~4 mm thick) sized to match the dimensions of a standard microscope slide (25 × 75 mm) and covered on one side with a standard size 2 (0.25 mm thickness) microscope glass slip-cover. This was done to allow for imaging using a variety of illumination techniques (imaging through glass), including DIC (differential interference contrast, also known as Nomarski IC). Approximately 0.3 to 0.5 ml of floc suspension was placed in the imaging chambers for every analysis.

Imaging of each specimen was done using several magnifications, typically including only some of the 10X, 20X, and 40X objectives. All specimens were analyzed using the phase contrast illumination method. This method was found to be the best for the current system for resolving the structure and the flocs.

Image capture was first conducted with a ProSilica (Allied Vision) GX2300 GigE camera via the Streampix software. This, however, was soon replaced with a combination of a Pulnix 1402CL camera and Matrox Inspector software because of the poor stability of the Streampix installation or software/hardware combination issues. The two cameras have similar characteristics and similar pixel sizes and resolutions. Figure 1 shows sample 1 under the 40X (PLAN APO) magnification.

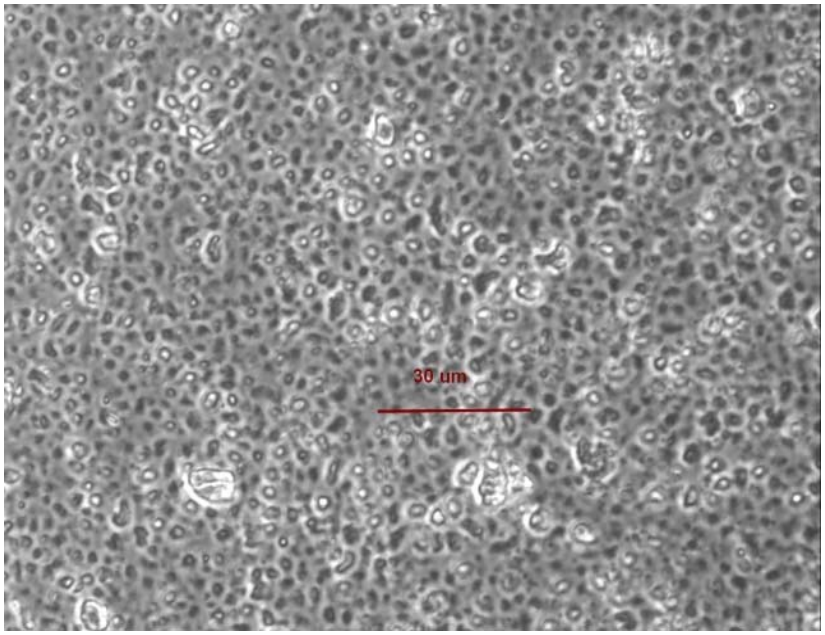

Fig. 1 – Sample 1 (0% X-gum, salinity: 0 PSU)

In this sample, we observe very little to no flocculation. Objects in the image appear to be the individual clay particles. Additionally, an unexpected Brownian-type motion was observed with many of the particles showing apparently random movements or strong vibrations from mean position with no apparent cumulative motion. Several single salt crystals are also visible in all samples examined. One such crystal can be seen in the lower left portion of Fig. 1.

A view of sample 2 is shown in Fig. 2 with the length of one of the flocs given for scale. Flocculation is noticeable under this minimal salinity, with some flocs even reaching an estimated size in the 20 to 50 μm range, as indicated in Fig. 2, but there is also much interstitial (if considering the flocs) material in the suspension, with many unattached individual particles. Additionally, the larger flocs that do form appear to represent only a loose packing of individual particles with noticeable gaps in between as well as multiple small appendages. These flocs have very limited to no observable spherical-like (or ellipsoidal-like) shape.

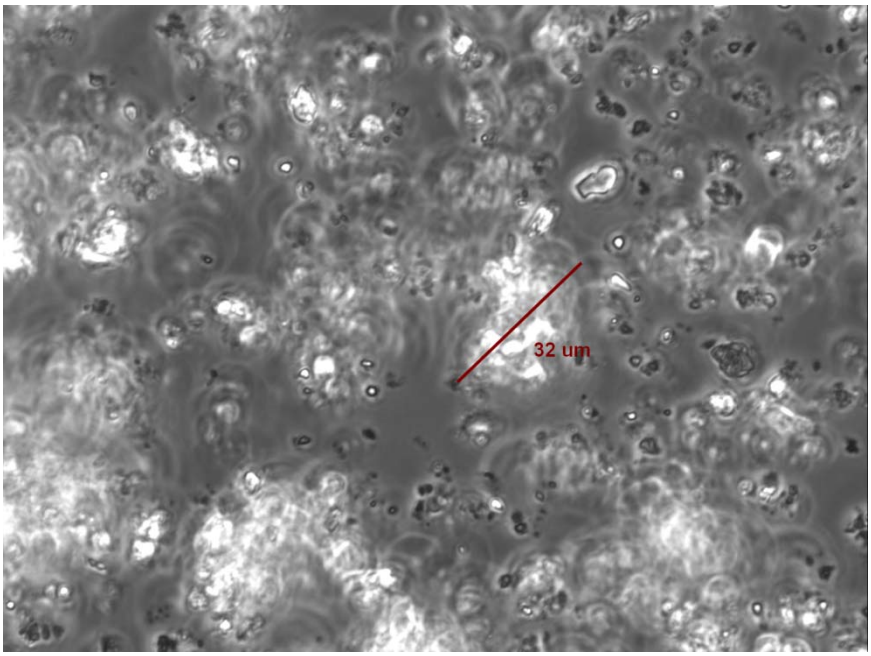

Fig. 2 – Sample 2 (salinity: 5 PSU, no X-gum) 40X, PLAN APO

Moreover, occasionally, and very rarely, some of these flocs seem to form somewhat larger "super-flocs" as shown in Fig. 3. These "super-flocs" are three to four times larger than the average floc; only one is visible in this sample, and it also has a significant structure in the vertical dimension. Because the microscope system used here did not have a calibrated Z-stack mechanism (distance-calibrated vertically moving focal plane), this floc was not imaged in the third dimension, and the volume occupied by the floc could not be quantified.

Figure 4 is a view of sample 3. This sample is similar, in general, to sample 2. Some increase in the estimated mean floc size seems to occur at this salinity with fewer individual particles (approximately 4 to 5 μm in size) and more flocculation, even if still into relatively small aggregates. The figure shows the size of a somewhat larger, among the typical, floc of 47 μm. There is still a significant amount of the interstitial unflocculated or weakly flocculated (small aggregates) material at this salinity.

Figure 5 shows sample 4. Dimensions of a typical floc are given in the figure. Another example is given in Fig. 6 with floc dimensions indicated as well. An example of an interstitial fluid with smaller flocs and floc fragments is given in Fig. 7. What is noticeable in all these images is that the interstitial fluid becomes freer of matter and a larger percentage of it is concentrated in flocs. The floc sizes generally get larger (on average) as the salinity increases, with 70 μm being an estimated mean size. The smallest size of individual particles observable also appears to increase to about 11 μm at this salinity. As before, even smaller particles (~4.5 μm) are also present, but their prevalence is diminished. This is even more obvious when looking under a relatively lower magnification, e.g., 20X. Figures 8 and 9 show the same sample 4 under this lower magnification. Representative (longer) dimensions of several flocs are shown in these figures. Also, Fig. 9 shows the very bottom of the imaging chamber, where one can see a number of flocs that have sedimented out of the suspension. This is a good representation of the diversity of sizes in any one particular sample, within which can be found flocs from as small as 24 μm, or even smaller, to as large as 229 μm. Similar sedimentation trends were observed in other samples of any substantial salinity (> 5 PSU), where much of the matter tends to accumulate at the bottom in a relatively short period of time after the sample is left motionless.

Another finding made during these observations was that the somewhat lower quality objectives (PLAN FLUOR vs PLAN APO) under this lower magnification appear to perform well, providing sufficient resolution without introduction of any undesirable optical effects (only Nikon objectives were used).

Next, we show results of observing sample 5 (20 PSU salinity, 0% X-gum) in Figs. 10 and 11. Although changes from one sample to the next involve only small changes in salinity (added 5 PSU), the trends observed earlier appear to continue. The average sizes of flocs continue to increase and the amount of interstitial material continues to decrease. Individually, the floc internal structure seems to be denser and more compact, with inter-particle attractive forces increasing due to increased salinity of the fluid. The internal structure of flocs also appears to vary. An example of two flocs with different internal structure is shown in Fig. 11. Here, one of the flocs possesses an apparently very dense internal structure (as visible under 40X magnification) and the other, just above it, appears to have a somewhat more amorphous composition. The first also seems very rounded in shape (near spherical) and the other (upper) has more irregular appendages and is somewhat less symmetric in shape. It is also possible that some of this observed structural effect is partially due to the different relative position of the current focal plane, i.e., the focal plane is passing through the middle of the lower flocs, revealing more of the internal structure, and closer to the outer edges of the second floc (upper) showing more of the surficial features. Another example of a floc with a rather dense internal structure is shown in Fig. 12.

It should be noted that judging the apparent density of the internal floccular structure (or degree of internal floc compaction) from visual observation alone may not always be most accurate. The illumination technique used here (phase contrast) also makes parts of the floc structure out of the current focal plane visible and these out of plane structures may interfere with our conclusions on the floc density. Ultimately, floc density can be addressed more accurately either with confocal microscopy technique or with specimen impregnation with resin (a technique not without its own drawbacks) and subsequent analysis of the thin sections with visible light microscopy or TEM (transmission electron microscopy). At this stage of our work, however, some preliminary conclusions may be made on the relative apparent density of the flocs. First, we only consider the part of the floc that is currently in focus, when comparing between the internal structures of different specimens. Second, the errors are minimized since the actual depth of focus for the objectives used herein was very small (0.30 μm for 40X, 1.10 μm for 20X, and 3.06 μm for 10X) compared with the dimensions of most flocs imaged. Refinements and actual quantifications of floccular density will be addressed in future work.

Next, we show the results for sample 6 (25 PSU salinity, 0% X-gum) in Figs. 13 and 14. All the trends that were noted before continue with this sample. In addition, the rate of sedimentation of the larger and denser flocs out of suspension also increases. This results in the situation depicted in Fig. 14 (shown under 20X magnification with a PLAN FLUOR objective), where the flocs are densely packed at the bottom of the imaging chamber, which is also the current focal plane in the figure. The flocs are mostly in direct contact with each other's outer layers, where one apparent distance is 10 μm (as shown in the figure).

Figures 15 and 16 show sample 7 (30 PSU salinity, 0% X-gum) under two different magnifications: 20X (PLAN FLUOR) and 40X (PLAN APO). The flocs continue to show dense internal structure, but it is difficult to tell if density has in fact increased from the previous value of the salinity of the fluid. One example of the denser flocs is shown in Fig. 16; it measures 127 μm and appears to consist of three individual sub-flocs that aggregated together and are now behaving as a single object during observation. While manipulators were not set during this stage of the investigation, rapid movements of the mechanical stage of the microscope indicated that this super-floc indeed moved as a single entity. Obviously, only precise force measurements of trying to separate the individual sub-components of this

aggregate could show if these are different from splitting of an otherwise uniform floc into sub-parts. This force measurement, which is discussed later in this report, was not available during this testing.

Examples of sample 8 (35 PSU salinity and 0% X-gum) are shown in Figs. 17 through 19. The flocs are generally similar to those in the previous sample and show the same trend in internal structure densification as well as the same dimensional distribution of flocs. Curiously, one may see a single large crystal (salt) in Fig. 18, comparable in size to one of the larger flocs. This has been noted in other samples as well. This salt crystal was probably formed due to drying after the sample aliquots were deposited into the imaging chamber.

The following paragraphs examine the next series of samples – 9 through 16 – that have the same salinity range as the sequence above but now contain 5% X-gum, in proportion to the clay mineral content by weight. The sample 9 solution salinity is zero. The general view under 40X magnification (PLAN APO objective) is shown in Fig. 20. Flocs appear to be completely absent. The suspension seems to have a rather uniform distribution of individual particles. No obvious sedimentation was observed.

Due to the testing system time availability limits, it was decided to examine only several selected samples in this group (5% X-gum as ratio of clay). Thus, sample 12 was chosen as the next sample for analysis. Here, two views of the material under the 40X magnification are shown, and give an example of material suspended in liquid (Fig. 21) and another of material sedimented to the bottom of the imaging chamber (Fig. 22). As is expected, denser (and larger) flocs tend to sediment faster and accumulate at the bottom. The sizes of the flocs are comparable, around 100 μm, but occasionally, one may find a very large individual floc (as in Fig. 22) with sizes of 370 μm, and some even larger. It was also noticeable that much of the matter has aggregated into flocs and that the fluid is relatively free of single unaffiliated particles. In this sample, sediment accumulation at the bottom of the vial was evident, after storage in the refrigerator overnight.

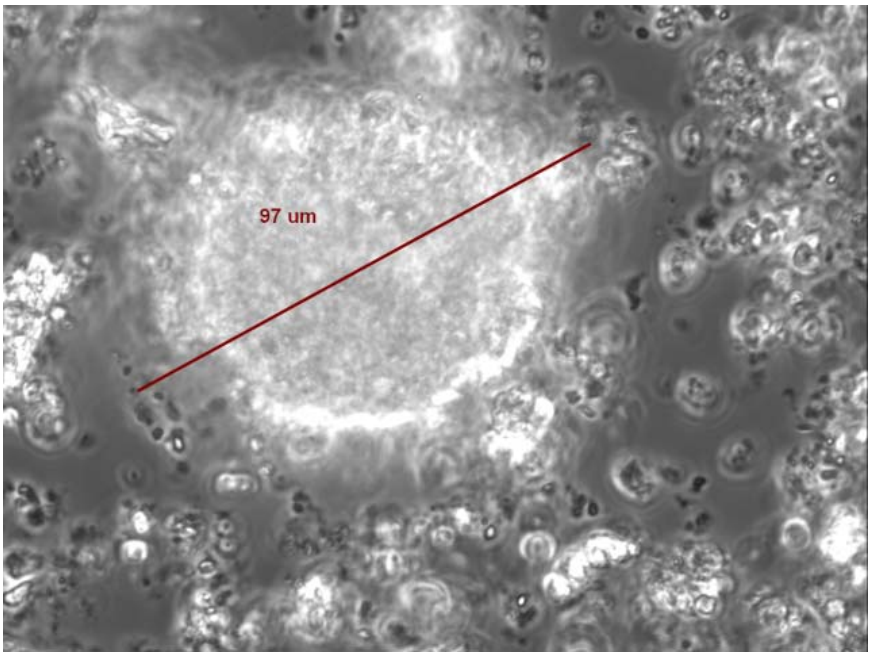

Fig. 3 – Sample 2 (5 PSU salinity, 0% X-gum) “Super-floc” 40X, PLAN APO

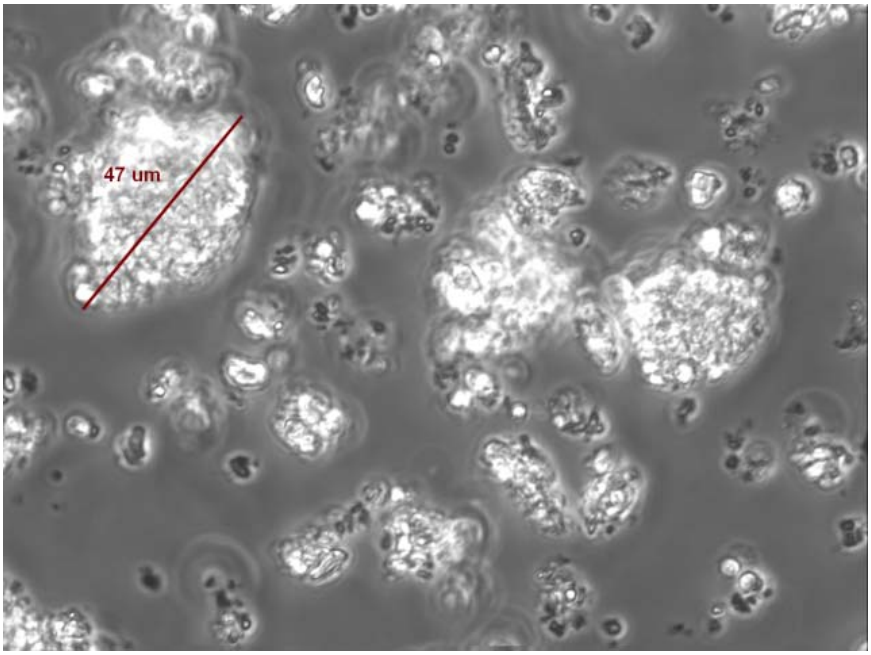

Fig. 4 – Sample 3 (10 PSU salinity, 0% X-gum) 40X PLAN APO

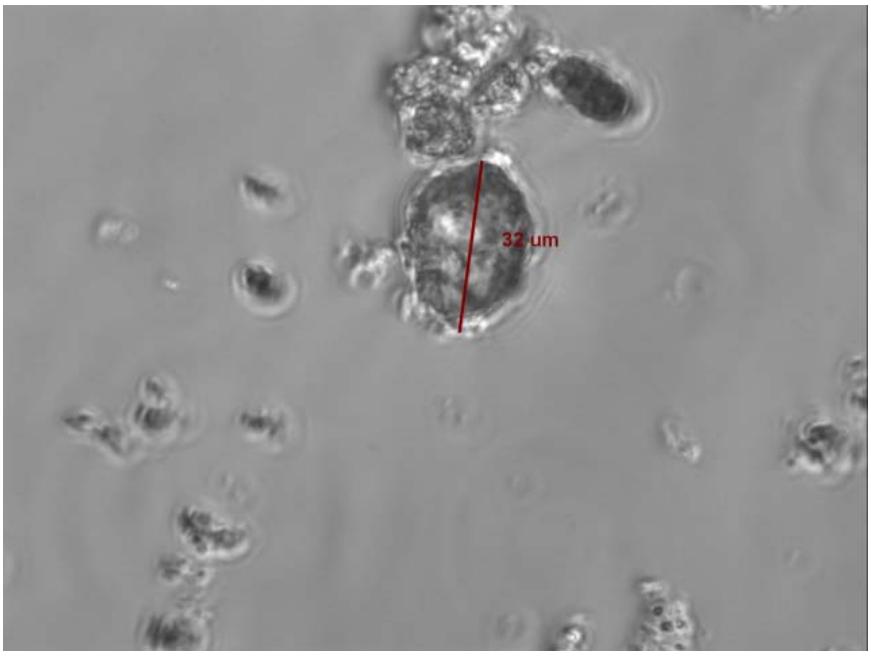

Fig. 5 – Sample 4 (15 PSU salinity, 0% X-gum), 40X PLAN APO

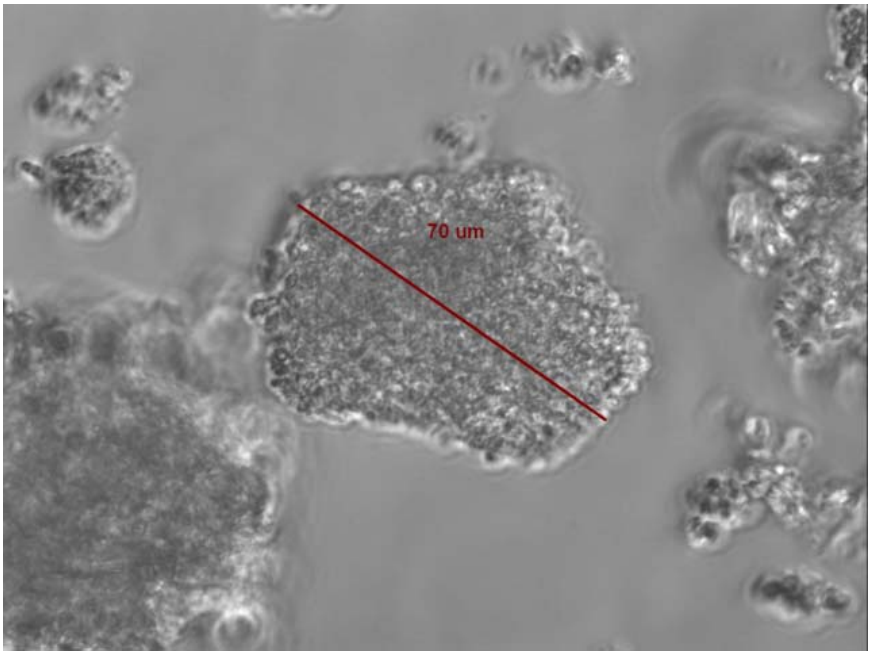

Fig. 6 – Sample 4, another typical floc, 40X PLAN APO

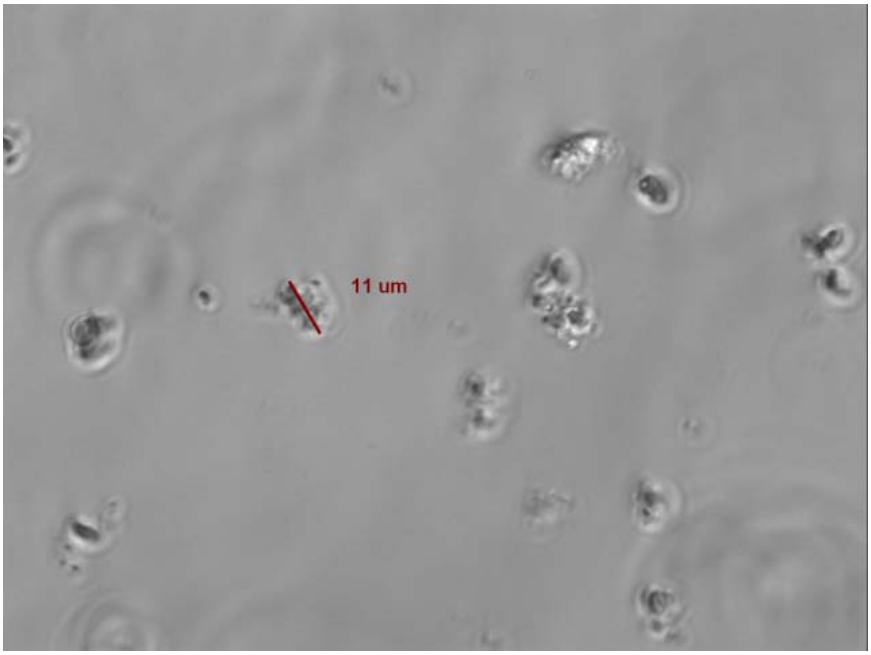

Fig. 7 – Sample 4 - example of a relatively matter-free interstitial fluid, 40X PLAN APO

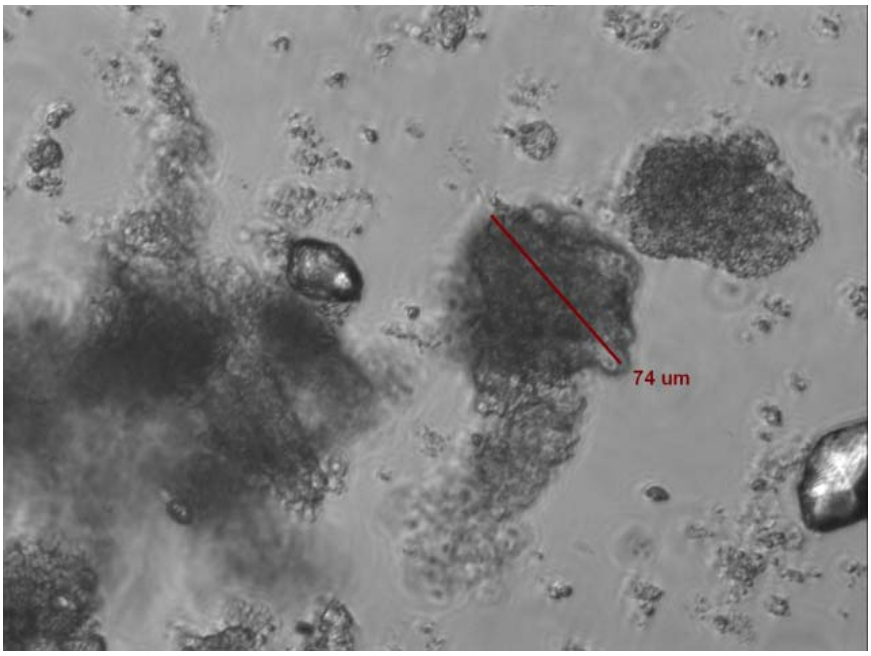

Fig. 8 – Sample 4, 20X PLAN FLUOR

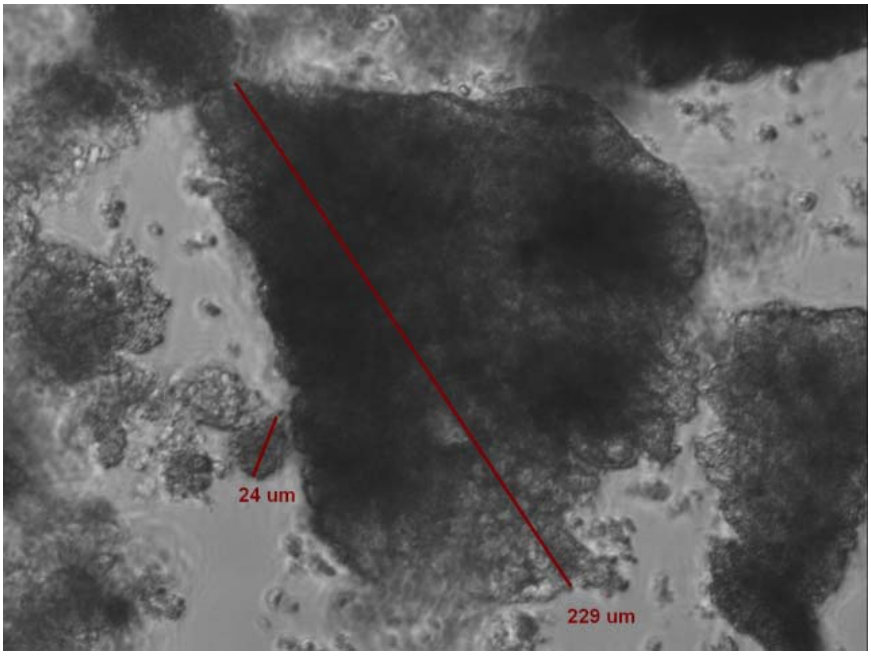

Fig. 9 –Sample 4 - bottom of the imaging chamber, 20X PLAN FLUOR

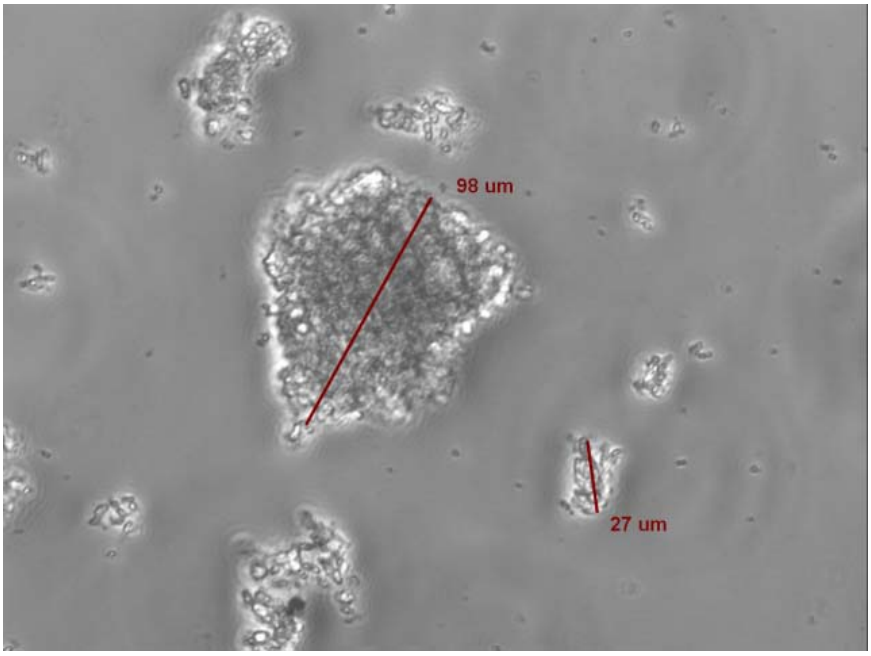

Fig. 10 – Sample 5 (salinity 20 PSU, X-gum: 0%), 20X PLAN FLUOR

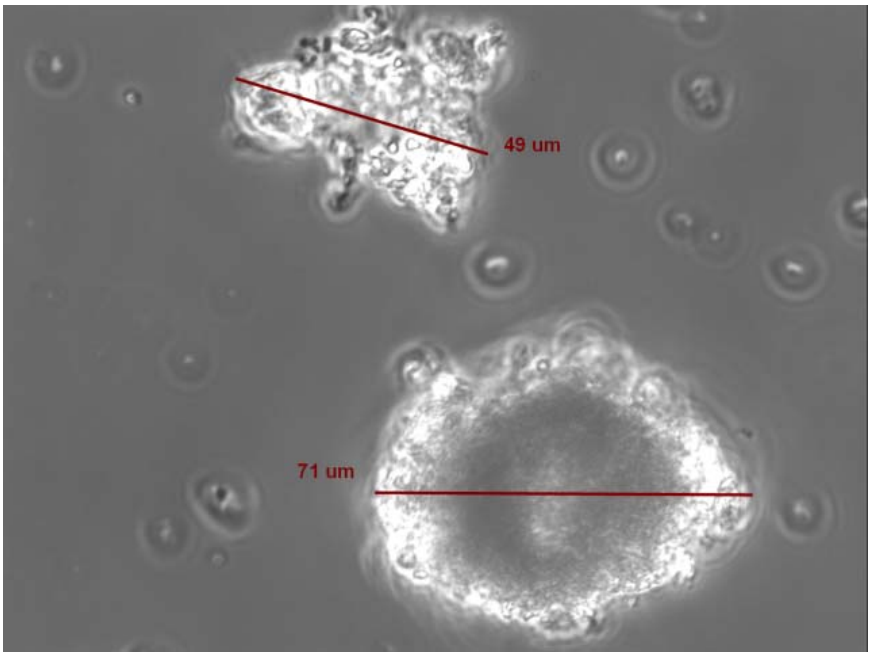

Fig. 11 – Sample 5 (salinity 20 PSU, X-gum: 0%), 40X PLAN APO

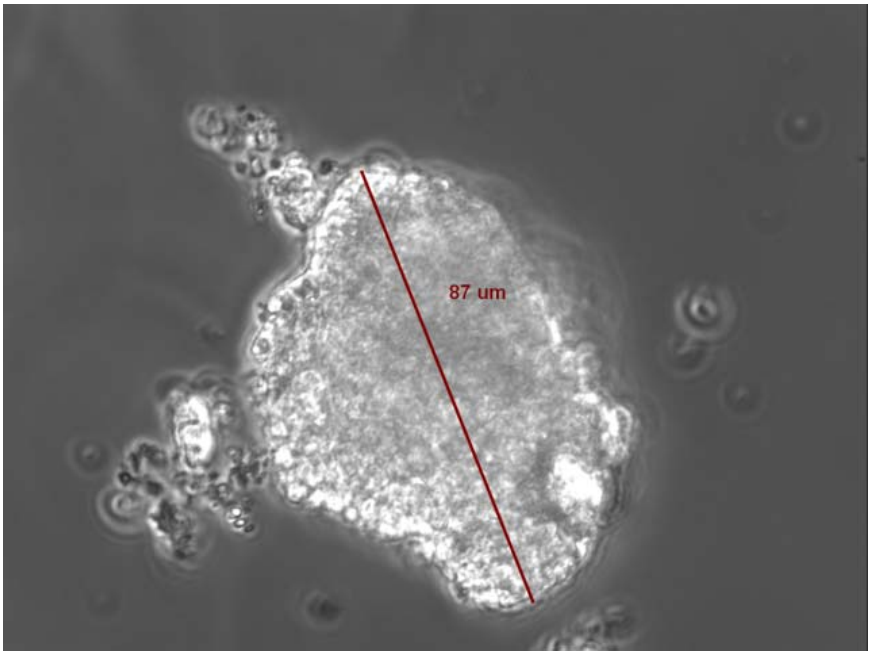

Fig. 12 – Sample 5 (salinity 20 PSU, X-gum: 0%), 40X PLAN APO. Example of a floc with a dense internal structure.

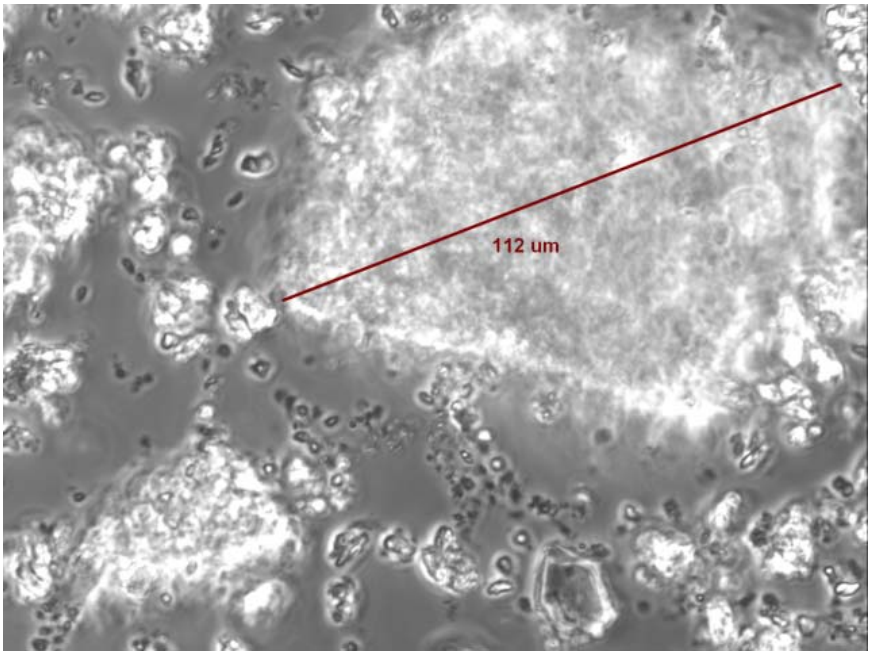

Fig. 13 – Sample 6 (25 PSU salinity, 0% X-gum), 40X PLAN APO

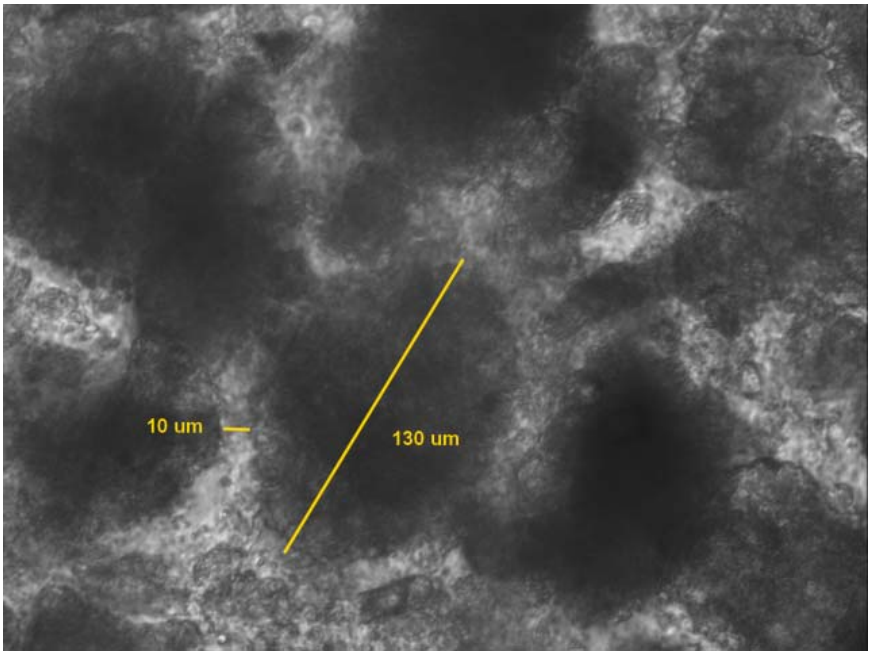

Fig. 14 – Sample 6 (25 PSU salinity, 0% X-gum), 20X PLAN FLUOR

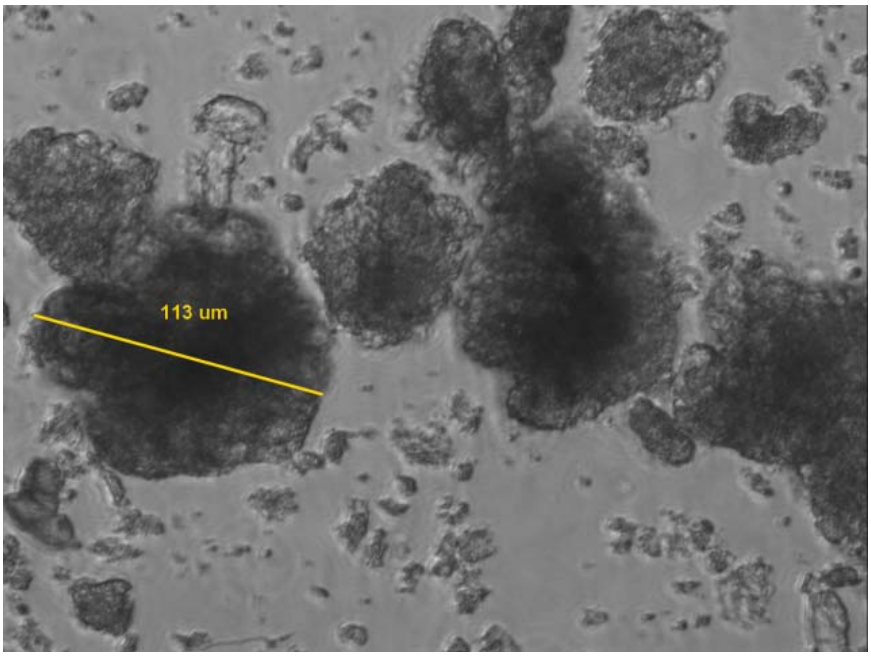

Fig. 15 – Sample 7 (30 PSU salinity, 0% X-gum), 20X PLAN FLUOR

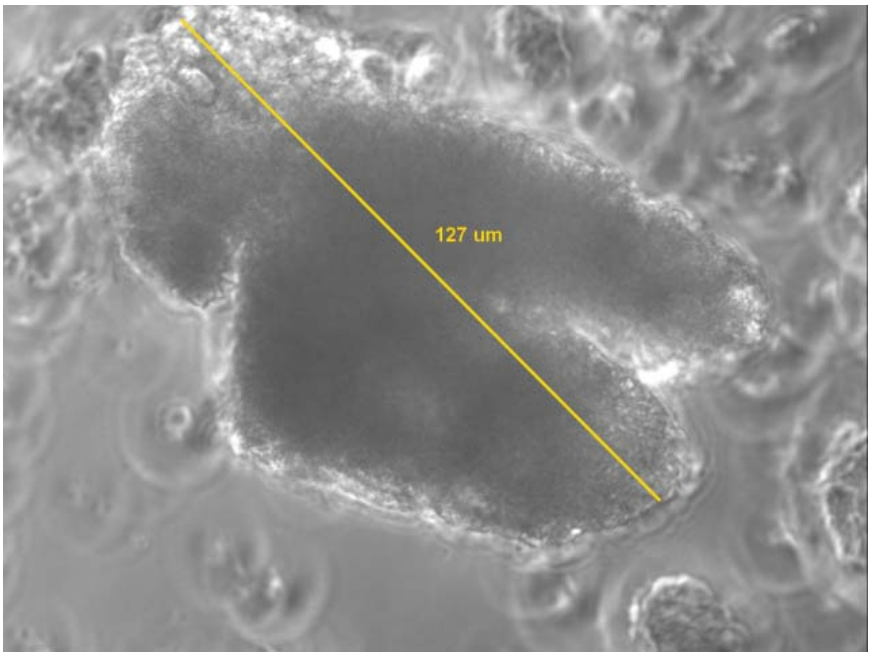

Fig. 16 – Sample 7 (30 PSU salinity, 0% X-gum), 40X PLAN APO. A compound dense floc.

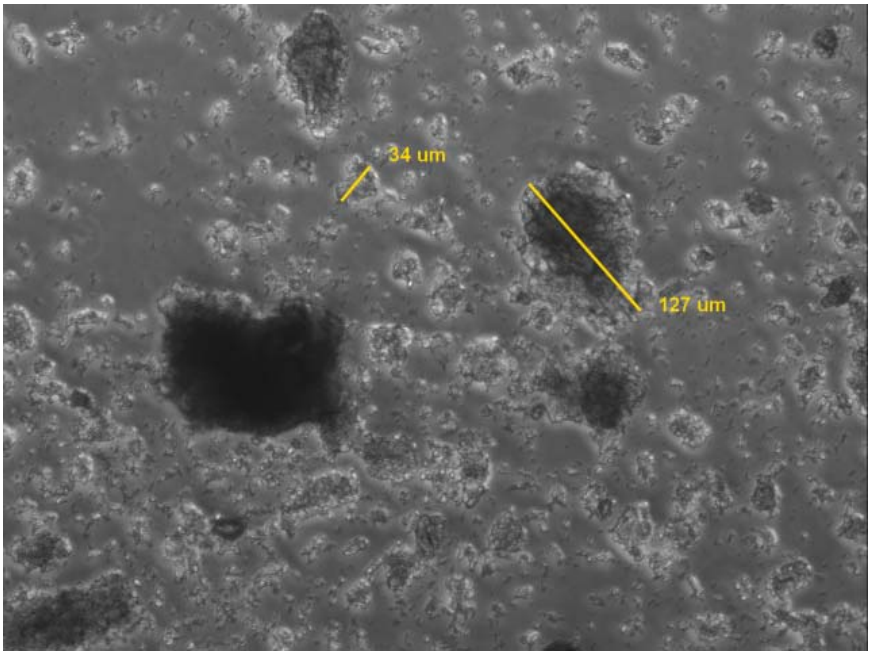

Fig. 17 – Sample 8 (35 PSU salinity, 0% X-gum), 10X PLAN FLUOR

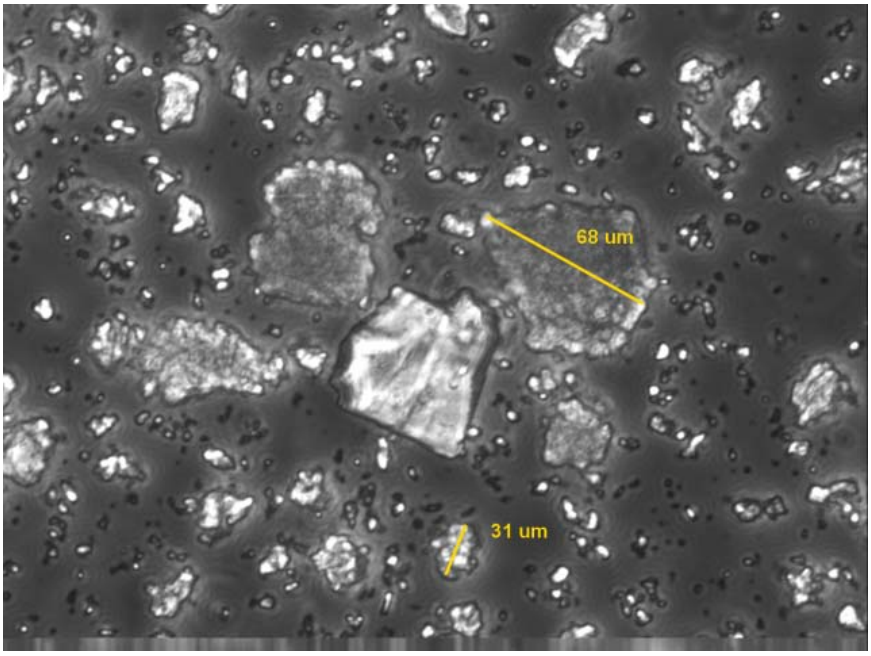

Fig. 18 – Sample 8 (35 PSU salinity, 0% X-gum), 20X PLAN FLUOR.
Example of smaller and larger flocs and a single salt crystal.

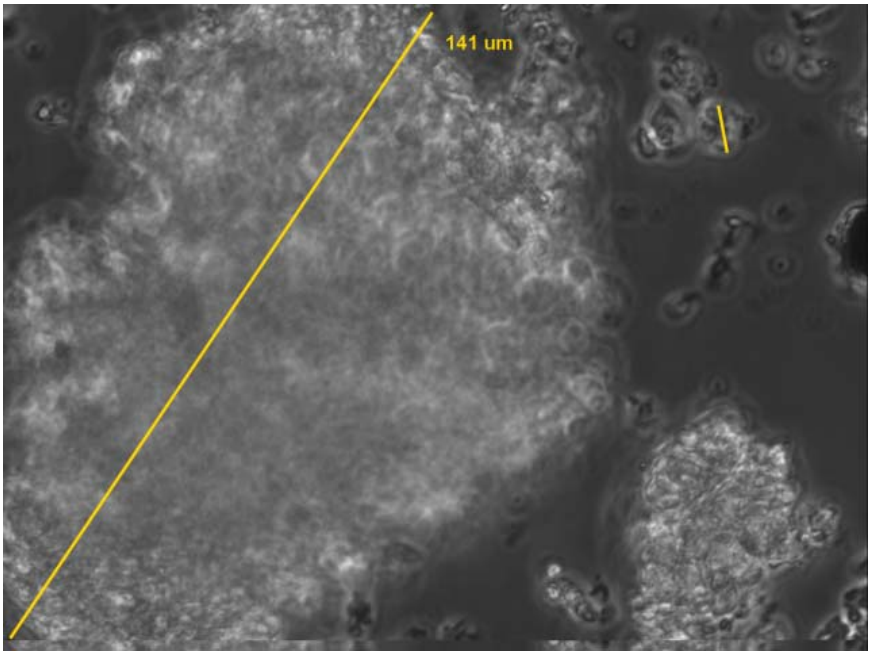

Fig. 19 – Sample 8 (35 PSU salinity, 0% X-gum), 20X PLAN APO.
A large floc with dense internal structure.

Additionally, a suspended particle gradient was also noted in the liquid above the sedimented mass. Since the storage vial was not imaged, we can assume that the particle gradation persisted with denser and larger flocs descending to the bottom. The flocs with presumably more amorphous internal structure (and therefore lesser density, as a result of the higher water content) and smaller flocs remained suspended longer at a variable distance from the bottom of the vial. This would be akin to the standard geotechnical hydrometer test of particle gradation for clays (colloidal component) and silts (granular fraction). While a rigorous particle gradation analysis is not intended here (nor is it possible), it would be reasonable to assume that this behavior may similarly be well represented by the Stokes' law, reinforced by the fact that many flocs have mostly spherical shapes.

Samples 14 and 16 are shown in Figs. 23 and 24, respectively. These samples contain 5% X-gum (as percentage of clay) and have salinities of 25 and 35 PSU, respectively. The trends observed earlier continue with the increased salinity. In general, the flocs appear to undergo little change in sizes in this range. The interstitial liquid is relatively free of smaller particles (elementary components) and strong accumulation of particles is occurring at the bottom of the imaging chambers. There were no readily observable changes in the floc sizes between these two samples. The range of sizes seems to remain relatively constant, with the majority of the flocs between 100 and 300 μm. The internal structure of the flocs, especially those close to the bottom of the imaging chamber, appears to be very dense, again, similar with previous findings and trends.

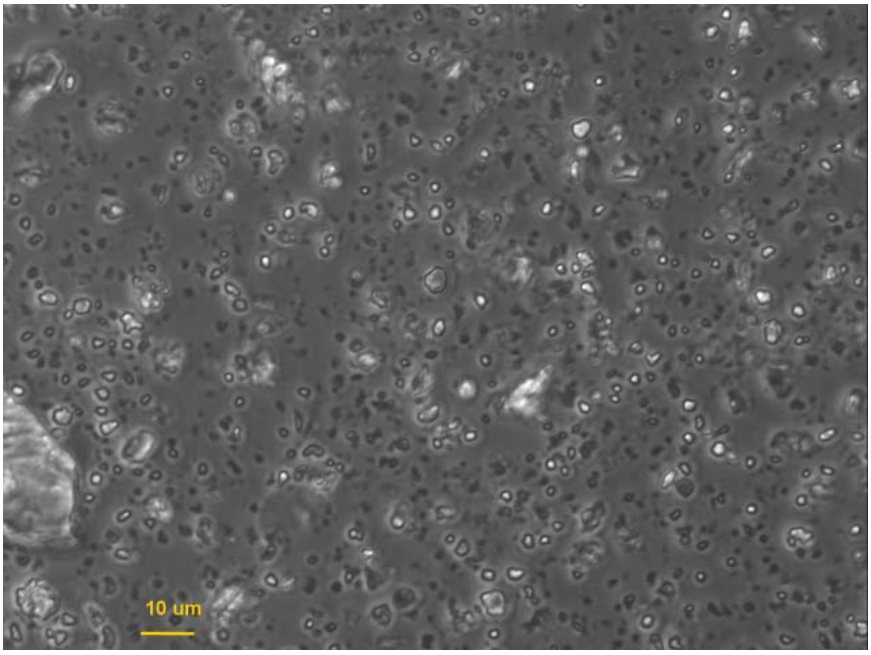

Fig. 20 – Sample 9 (0 PSU salinity, 5% X-gum to clay ratio), 40X PLAN APO

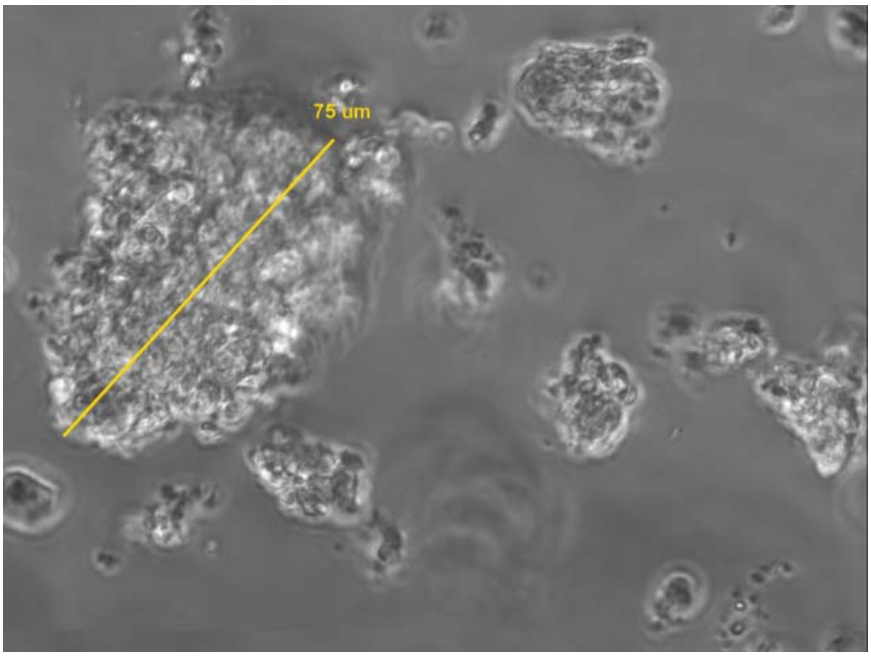

Fig. 21 – Sample 12 (15 PSU salinity, 5%X-gum to clay ratio), 40X PLAN APO, flocs in mid-suspension

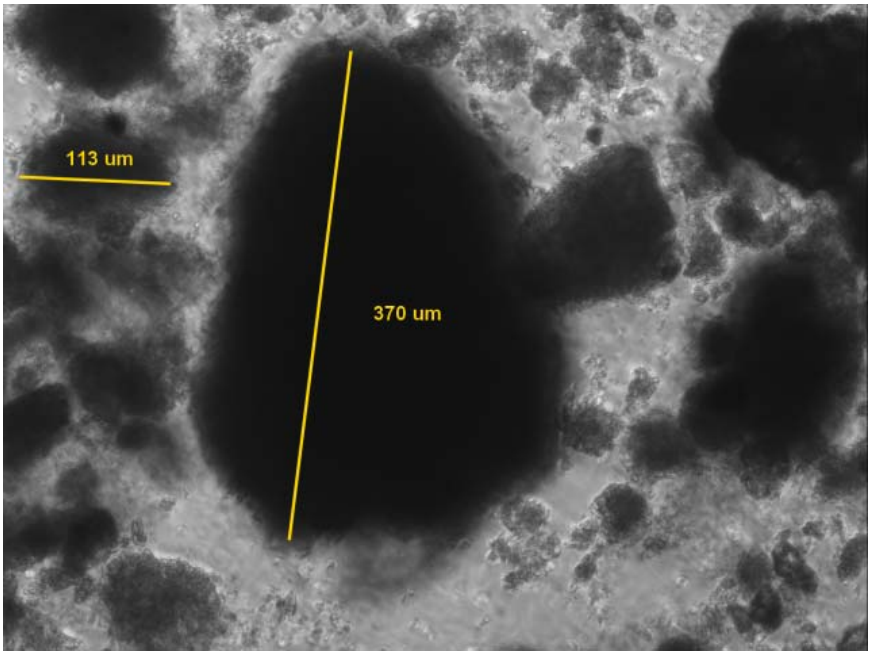

Fig. 22 – Sample 12 (15 PSU salinity, 5%X-gum to clay ratio), 40X PLAN APO, flocs at the bottom of the imaging chamber

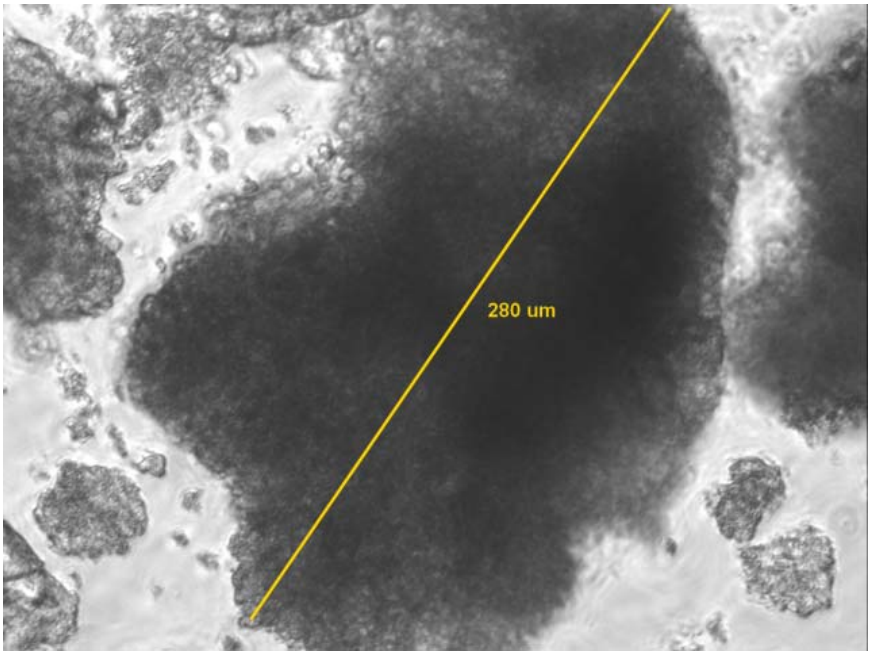

Fig. 23 – Sample 14 (25 PSU salinity, 5% X-gum to clay ratio), 20X PLAN FLUOR

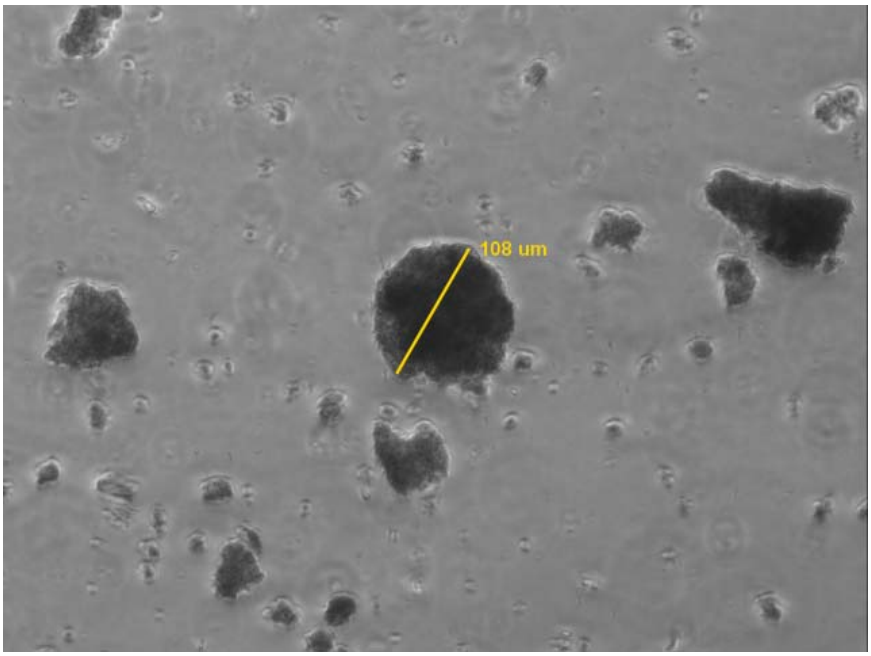

Fig. 24 – Sample 16 (35 PSU salinity, 5%X-gum to clay ratio), 10X PLAN FLUOR, flocs suspended in fluid

We now examine a few samples of the 10% mixture of the X-gum (as relative to the clay component) at different salinities. The first specimen in this series, sample 17 (0 PSU salinity, 10% X-gum relative to clay), is shown in Fig. 25. Little to no flocculation is evident as only individual particles on the order of 3 to 5 μm or only very small flocs of less than 10 μm are present. Figure 26 shows an example of the largest floc found – 19 μm. Most of the matter appears to be highly dispersed throughout the liquid with no obvious accumulation at the bottom of the imaging chamber. Sample 19 (10 PSU salinity, 10% X-gum relative to clay) is shown next in Figs. 27 and 28. As before, the largest size of the flocs found free-floating in the liquid (Fig. 27) is smaller than those that sedimented to the bottom of the imaging chamber (Fig. 28). In this case, the largest floc found suspended in the liquid was 96 μm, and the largest floc found on the bottom of the chamber was 272 μm in size and had an apparently denser internal structure. In this sample, much of the material was found sedimented to the bottom, some forming large clusters of flocs, almost merging together, with only a small amount of interstitial liquid in the spaces between them.

The final sample (21) examined here is shown in Fig. 29 (20 PSU salinity, 10% X-gum, relative to clay). The image shows a wide variety of flocs at the bottom of the imaging chamber, varying in size from 40 μm, and even smaller, to much larger flocs, e.g., 228 μm. One distinction at this salinity vs the lower salinities (but the same X-gum content) is that the range of the floc sizes appears to be wider, incorporating particles of small, medium, and large sizes. It is possible that the larger X-gum content is preventing the rate or the degree of floc formation to some extent, where the individual particles need to overcome the viscous drag forces generated by the polymeric compounds in the liquid in order to flocculate, in response to the change of the particle surface potentials caused by the increased salinity. With less X-gum content, this process appears to occur faster and more completely, resulting in the larger portion of the matter accumulating into aggregates of larger size, resulting in a more uniform size distribution of flocs. In this work, the issues of time dependence on flocculation were not explored systematically, so the amount of time it takes a sample at the same salinity but a higher polymer content to flocculate to a comparable floc size distribution (if attainable at all) is not known. This could be a subject of further testing and a more systematic analysis in which rates of flocculation and the resulting floc size gradation can be related to the viscosity of the interstitial fluid, measured with a rheometer, with the certain amount of X-gum (or other polysaccharide) in it.

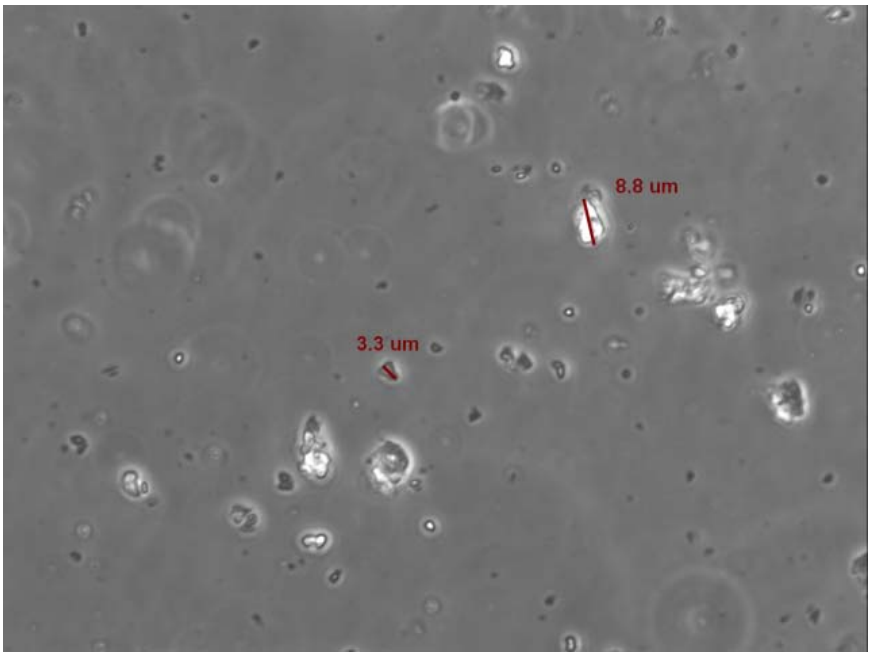

Fig. 25 – Sample 17 (0 PSU salinity, 10% X-gum relative to clay), little to no flocculation, 40X PLAN APO

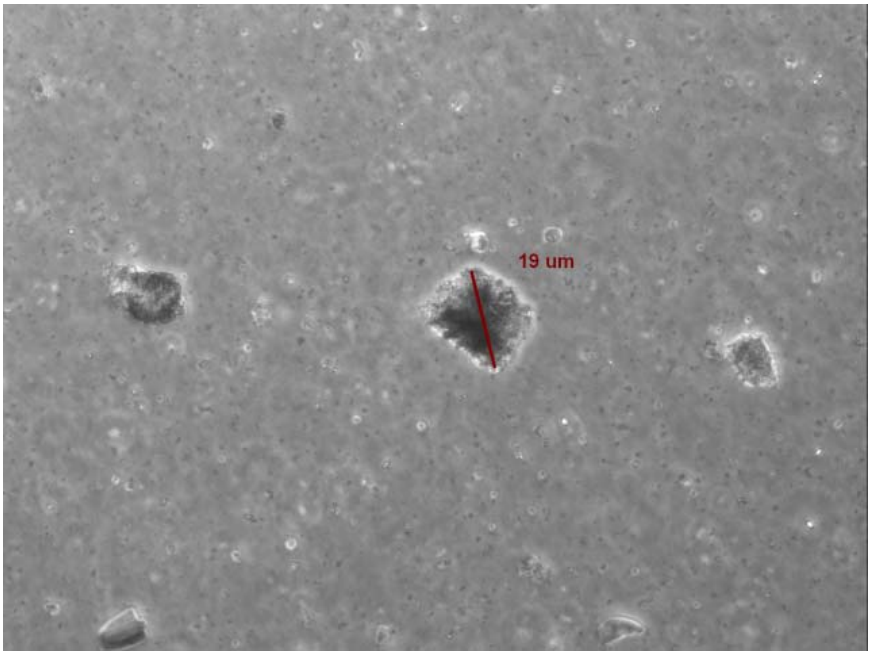

Fig. 26 – Sample 17 (0 PSU salinity, 10% X-gum relative to clay), largest floc observable, 40X, PLAN APO

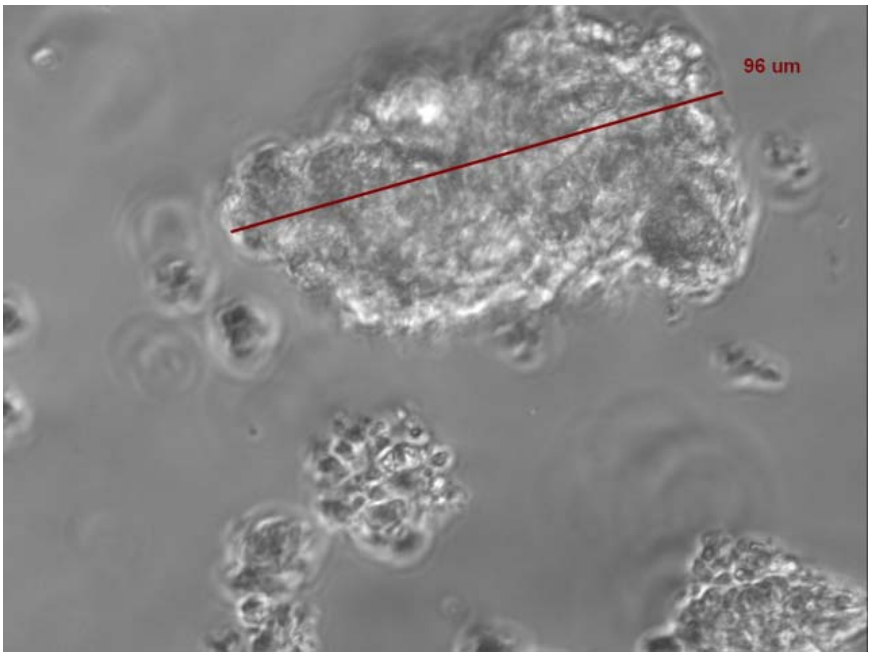

Fig. 27 – Sample 19 (10 PSU salinity, 10% X-gum relative to clay); one of the largest flocs observable and free-floating in the liquid; 40X, PLAN APO

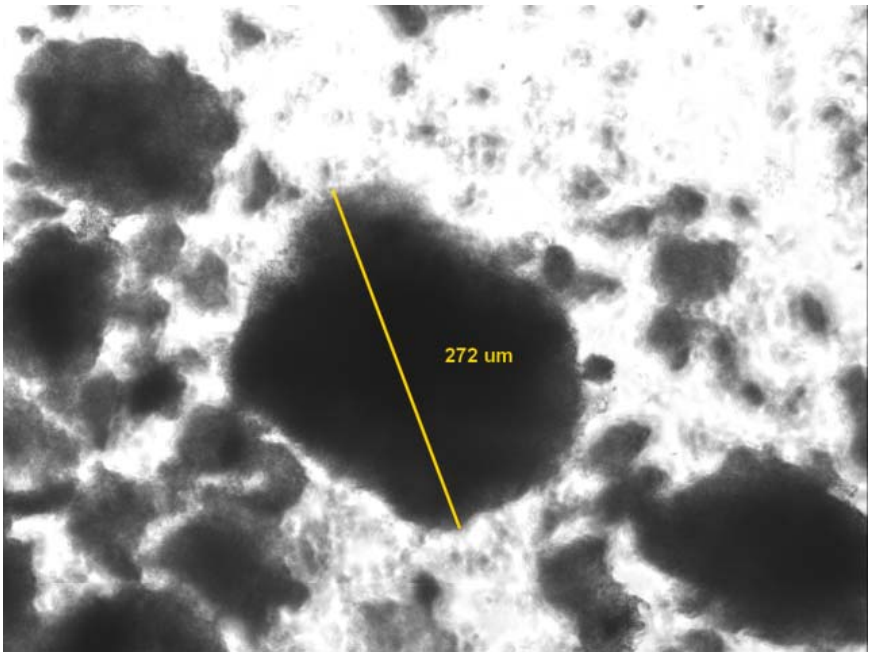

Fig. 28 – Sample 19 (10 PSU salinity, 10% X-gum relative to clay); one of the largest floc observable at the bottom of the imaging chamber; 10X, PLAN FLUOR

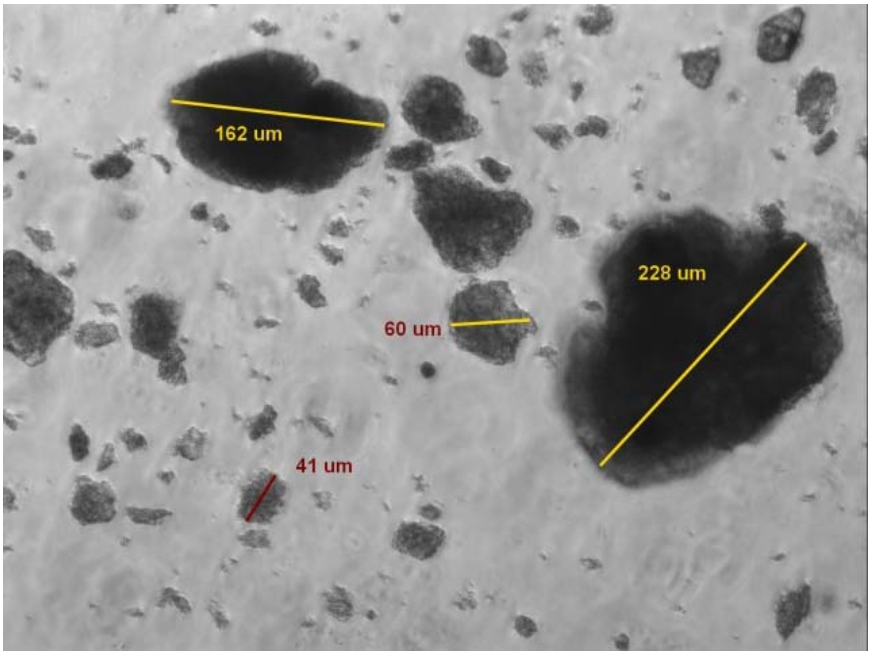

Fig. 29 – Sample 21 (20 PSU salinity, 10% X-gum relative to clay); a variety of flocs at the bottom of the imaging chamber; 10X, PLAN FLUOR

3. MICRO-PIPETTES

In this section, a description of the micro-pipettes is given, including pipette drawing, shaping, and force-displacement calibrations. The equipment used included a micro-pipette pulling device from Sutter Instrument Co. (P-97) and a Narishige micro-forge (MF-79) used for pipette shaping and bending and in the force calibrations. Currently, these device models are not available, but have been superseded with newer and slightly updated replacements by the same companies. Most of the improvements are minor and would not change the fundamentals of the procedures and methods on all aspects of pipette production.

The pipette drawing is generally conducted on machines with controlled heat delivery to the heater element (the filament), controlled rate of pipette ends motion, and a certain choice on the original glass tubing selected for drawing. The setup currently used at the Biolab of the University of Oakland includes procedures and drawing programs, as well as the stock glass tubing used, as to produce micro-pipettes with very long and thin tapers, where the diameter of the very tip could be on the order of 10 μm or less (and as little as 2 to 3 μm) and a relatively long section of the pipette with an approximately constant diameter. In general, the ability to produce micro-pipettes with constant diameter is difficult to achieve, as it is not controlled directly, but still depends on the same factors of temperature, rate of pull, and the dimensions of the initial glass tubing. Trial and error approach is generally used from an initial starting (device programming) point of a certain combination of these factors, from which the adjustments are made until the desired shape and size of the micro-pipette has been attained. During these trials, we did not have the full range of glass tubing and filament shapes to fully explore the parameter space and to determine which combination is best suited for floc manipulation of a certain size.

The ends of the micro-pipettes, necessary for floc attachment under controlled (small) suction and manipulation, need to be comparable to the sizes of the flocs being manipulated. The amount of suction applied needs to be minimal but sufficient to allow secure floc handling and floc testing without detachment from the end of the pipette. The amount of suction applied and the internal opening of the micro-pipette needs to be such that the floc matter will not be affected by the suction. Given the floc sizes explored in the previous section, the ends of the pipette needed for both floc holding and floc manipulation would need to be in the range of between 30 and 50 μm (and perhaps as high as 100 μm for larger flocs), depending on the actual size of the floc under manipulation.

Measurement of floc strength may be best accomplished when one end of the floc is held steady with a larger and stiffer pipette, while the other side is attached to a movable pipette that is flexible enough to register displacement under applied load as a result of a controlled movement of a manipulator. If the flexible manipulated pipette is calibrated for the force-displacement of a particular point near its end, visible throughout the procedure, the load imposed under these conditions can be measured, similar to Yeung and Pelton (1996).

The types of micro-pipettes best suited for the holding function are also called “patch-clamp” pipettes in biological sciences and are used, similarly, for holding various elementary biological structures. Both the holding and the manipulating pipettes need to be manufactured in such a way as to preserve the internal opening so that the vacuum can be applied.

Production of patch-clamp style pipettes is typically not difficult, as no bending is required, and only some control over the tip of the pipette may be necessary for those with the very large diameter, so that the jagged and uneven edges are avoided or smoothed over, typically by using a micro-forge. In this work, we used several pipettes drawn to specification previously used by the Biolab of the Oakland University. Long tapers were broken off at a point where the overall pipette diameter and resulting apparent stiffness of the remaining cantilever was considered sufficient for holding purposes. No specific stiffness measurements were made for patch-clamp pipettes, as only preliminary manipulation examples were sought during this experiment.

Micro-pipettes designated for force measurements need to be different from the holding pipettes. The flexural rigidity of these pipettes needs to be such that the forces expected during the floc strength testing would result in displacements, as a result of bending, that are (a) large enough to allow for sufficient resolution in measurements and (b) not too large as to result in manipulator out of range without generating sufficient force to achieve the desired floc break-up. Many options for pipette pulling were not available during the experiments, i.e., different filament shapes and initial glass tubing of different combination of internal and external diameter. Thus, pipettes typically used at this particular laboratory of Oakland University were used. These had long and relatively constant diameter sections, tapering down to tips as small as several microns. Several were selected for testing and were broken off to attain a tip of 10 μm or larger. Pipettes with this small a diameter would be poorly suited for manipulating larger flocs (e.g., 200 μm) but were selected here nonetheless for possible testing of smaller flocs and as a proof of concept, in the absence of significantly better options.

In order to produce a force-displacement relationship for the pipettes intended in tensile strength measurements of the flocs, a calibration is required such that the force (and suction during test) is applied normal to the long axis of the pipette (its long section). The pipette therefore has to have at least an L-shaped geometry, as was also used by Yeung and Pelton (1996), so that this method of force application and displacement measurements is possible. This involves a process of bending the pipette into a right angle using a micro-forge. It is done by temporarily heating the glass of a drawn pipette in a very specific manner, dependent on the filament temperature, initial filament position, rate of advance toward the heated region of the pipette, and the rate of withdrawal. This localized application of heat

generates a thermal stress field within the glass that bends the tubing. It is also dependent on the initial dimensions of the pipette that is being heated. Heat is turned off (or heater element is rapidly withdrawn) when the desired bend has been achieved. An important attribute of this bending in our case is not to allow the glass to fill in, melt, or otherwise close or obstruct the inner diameter of the pipette, so that suction can still be applied during testing for floc attachment. This proved most difficult to accomplish with the range of the glass tubing tested and the available pre-drawn micro-pipettes. Bending pipettes with tapers on the order of 10 μm is relatively easy, where the tip of the pipette deflects away from the heater element during the active heating phase, which occurs in relatively rapid manner due to the small amount of glass in the heated area. For larger diameter pipettes, e.g., with tapers of 40 μm or larger, the direction of the bend does not appear to be easily controlled. Most often, the tip is bending toward the heater element, which also needs to be at a higher temperature to facilitate quicker bending and to prevent the glass from closing its inner capillary. Unfortunately, during the limited number of bending attempts that could be completed within the scope of this small preliminary study, no satisfactory result could be obtained on the thicker pipettes. Suitable combination of temperature of the filament, initial glass dimensions, and heat application modes was not found. At every attempt, the resulting micro-pipette, even if bent to the desired right angle, would close the internal capillary, preventing any vacuum application during actual floc testing. The heat application methods were followed approximately correctly and to the best of the given equipment's capacity. Consultations with the experts from Sutter Instrument Co. revealed that the optimum initial glass sizes and best filament shapes were not used in our trials. According to the Sutter technical support personnel, the new Narishige micro-forge device, currently available, has improved capabilities on the accuracy of heat application and filament movement with respect to the tip of the pipette that would allow for the necessary bending to be performed as desired. Sutter, also the producer of the pipette pulling machines, can provide initial training in the art of pipette drawing and bending. Micro-pipettes of small tip diameters of about 10 μm were drawn and bent with success, with internal capillary preserved. This capillary, however, narrowed and even though visibly open, was apparently too small in diameter for the vacuum to overcome the surface tension forces of the fluid and allow proper application of suction. Several other pipettes were drawn and bent using a series of variable rates of heating and filament approach. Some of these yielded acceptable bends of close to the right angle. The internal capillary, however, was either obviously closed or likely closed as a result of the procedure. Given the limited time, no optimal procedure was found.

In view of these results, only simple manipulation was conducted as no flocs could be pulled apart by application of forces in opposite directions due to the inability to apply suction reliably to one of the pipettes (flexible, force-measuring).

Force-displacement calibrations of micro-pipettes were the next important item on the agenda. Here, we attempted the calibrations of two different geometries: bent (right angle) and straight. First, a procedure adopted by Schmitz et al. (2000) was followed. In it, polystyrene beads of two different available diameters (45 and 90 μm) were attached to the tips of the micro-pipette using static electric charges (as shown in Fig. 30).

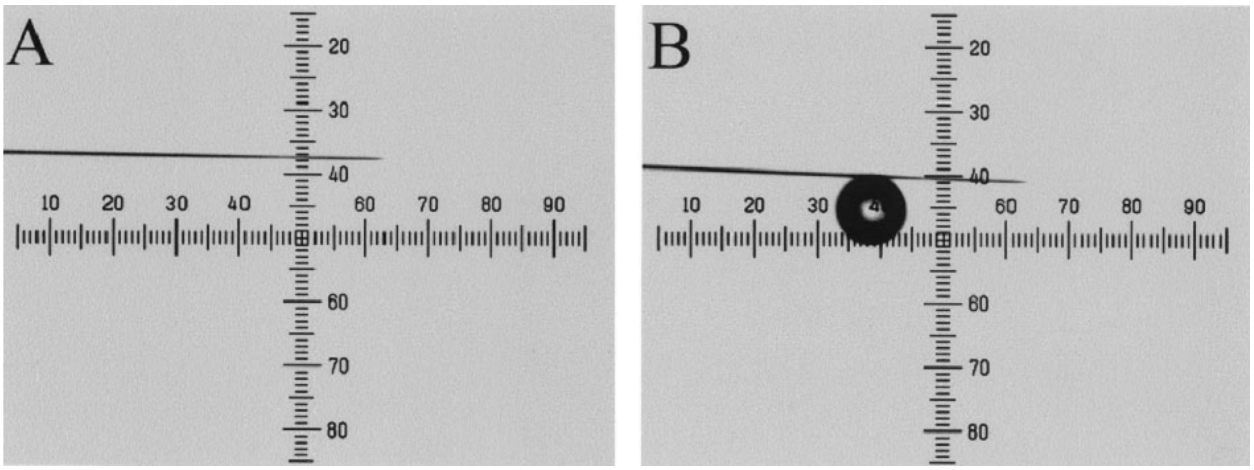

Fig. 30 – Polystyrene bead method of force calibration of micro-pipettes (after Schmitz et al. 2000)

The picture is taken through the microscope that is a part of the Narishige micro-forge. The unique property of this microscope is that it is oriented horizontally, allowing for the observation of the displacements as a result of gravitational loading on the micro-pipette cantilever. This type of measurement is most accurate, as it relies on the knowledge of the density of the bead, which for materials such as polystyrene can be known precisely, and the actually measured diameter of the spheres. Additional beads can be attached for greater deflections, as was done by the authors. In the Schmitz study, an averaged position of the combined weight of the beads was used, assuming that the differences in position of the beads along the cantilever were small compared with the total length of the cantilever beam (thin portion of the drawn pipette). In case of the bent pipette considered here, the test was conducted with the bent portion pointing straight down. We then attempted to attach the beads to this section of the pipette, thus maintaining the distance from the point of the force application to the fixed part of the pipette at a constant value. This method would relate to the force at the tip directly. If several beads are attached to the cantilever at different positions along the pipette (and comparable to the length of the cantilever itself), the summation of the forces needs to be related to an equivalent force, as if it were applied at the very tip of the cantilever, and producing the same deflection. This is necessary as during the actual test with flocs, the force is only applied at the tip.

Pipettes of small (and relatively constant) diameter of the active part of the drawn micro-pipette – portion undergoing flexing, as those used in Schmitz et al. (2000) – can be calibrated successfully with single or only few smaller beads (out of available 45 and 90 μm diameters), producing sufficient deflections to span the range of forces necessary for tests. This procedure was first attempted for a pipette with a tip of about 4.4 μm and using the larger (90 μm) polystyrene beads to attain larger forces. Two loadings were made: a single bead was attached near the tip of the pipette, and then a cluster of four beads was attached in similar fashion. The density of the polystyrene beads was 1050 kg/m^3. The results of this calibration are shown in Fig. 31.

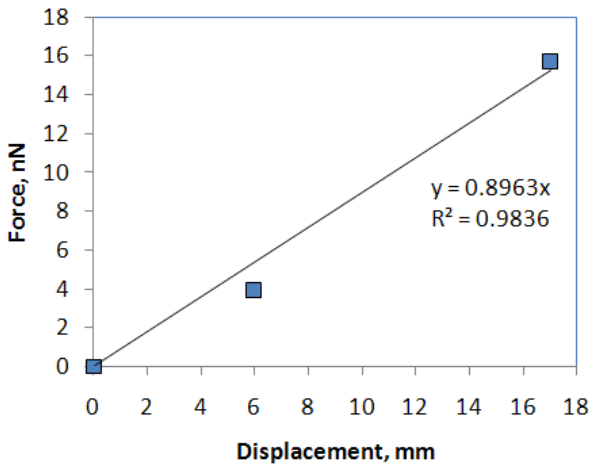

Fig. 31 – Calibration of straight pipette 1 with polystyrene beads of 90 μm in diameter

A difficulty of attaching the beads was observed. In order for the beads to attach to the micro-pipette, the beads were rubbed on a wool-like material to impart to them a static electric charge. Additionally, the pipette itself was similarly rubbed. This procedure was found to be rather perilous due to the very long and thin cantilever of the drawn micro-pipette, resulting in easy breakage of the pipette. Even though the calibration curve is rather linear, it only contains two meaningful points and further loading was not possible as attaching additional beads (in excess of four) was not successful.

Comparatively larger forces are expected during our planned tests on larger flocs (order of 100 μm) and thus larger diameters of the tip will be needed to accommodate these floc sizes and hold them securely, as well as apply suction and manipulate these flocs without (as much as possible) any damage to their structure. This damage is expected if manipulation is done with very small pipettes (tips of several microns OD) and higher suction, anticipated to hold the larger flocs securely.

A second calibration attempt was undertaken on another micro-pipette (1 mm OD, 0.78 mm ID) with a bent section. This section was approximately 0.7 mm long and the very tip of the pipette had an outer diameter of 8 μm. The thin (drawn) part of the cantilever was approximately 26.5 mm and had an average diameter (outer) of approximately 13 μm. There was some detectable diameter change from the tip of the cantilever to the end of the thin section. This change was sufficiently small that the entire length of the thin section of the micro-pipette could be reasonably considered constant in diameter.

Bead calibration method was attempted again on this pipette, as before. Again, it was discovered that placing a select number of beads on the bent tip of the pipette was very difficult. Imparting a static charge to the pipette without breakage was difficult too, resulting in a degraded ability to transfer the beads to the pipette tip. Due to this persistent difficulty, another calibration method was attempted. This method was first described by Yoneda (1960). In this original work, small pieces of copper wire with known diameter and measured lengths were bent into a horse-shoe shape. Knowing the density of the material and being able to measure the actual dimensions of the cut pieces accurately allowed for an easy calculation of the total weight of each of these weights. This method was chosen as an alternative to the bead calibration technique. In the absence of a copper wire, a piece of a titanium filament was used instead. The tabulated value of the density was used (2145 kg/m^3), and the dimensions of a small cut piece were measured. The diameter of the wire was 100 μm and the length 1105 μm. This piece of wire was bent into a horse-shoe shape, a feat not easily achieved with platinum. Instead of having multiple small weights that could be added at (or near) the tip of the pipette, which would make for a simple and

straight-forward calculation of the force-displacement curve, a single weight was moved along the micro-pipette, thus producing different deflection of the tip.

The theory of beam bending can be used then to calculate the relationship between the force at the tip of the pipette to that at any other location along the cantilever. In the simplified case of a constant flexural rigidity (*EI*, where *E* is the Young's modulus, and *I* is moment of inertia of the cross-section), made based on the assumption of a constant diameter of the micro-pipette, the standard solution of the beam equations can be used.

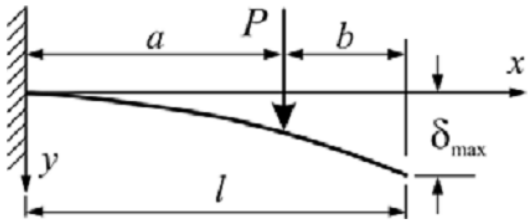

Fig. 32 – Cantilever beam with the displacement- and moment-fixed support on the left end; δ - deflection of the tip, *P* – load.

Figure 32 shows the variable definitions for deflection of a cantilever beam with moment-fixed and displacement-fixed support on one end. We are looking for an equivalent force that, if applied at the end of the cantilever, would produce the same deflection as the force applied somewhere along the length of the beam. We have the following equation for the maximum deflection (e.g., Timoshenko 1940), when the force is anywhere along the beam:

$$d_{\max} = \frac{Pa^2}{6EI}(3l - a) \tag{1}$$

If we designate the equivalent force acting at the tip of the cantilever as P_e, we can write an equation for the tip displacement as follows:

$$\frac{Pa^2}{6EI}(3l - a) = \frac{6P_e l^2}{3EI}, \tag{2}$$

from which the equivalent force can be derived as:

$$P_e = P\,\frac{a^2(3l - a)}{2l^3}. \tag{3}$$

Using Eq. (3) now allows for calculating the equivalent force and calibrating the micro-pipette. Calibration was conducted recording deflections from five different positions of the weight along the length of the cantilever. The resulting calibration curve for the tip force is shown in Fig. 33.

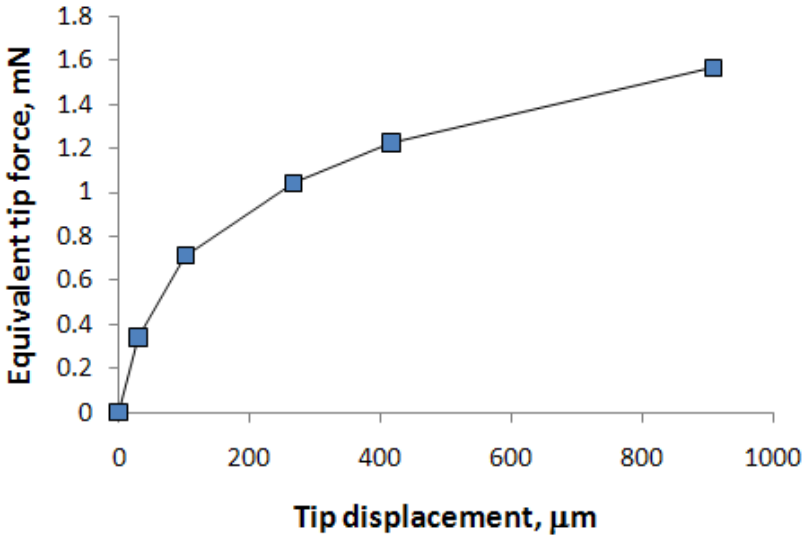

Fig. 33 – Calibration curve for the equivalent force using a single weight and multiple positions along the length of the cantilever

The technique presented here seems preferable to the bead-based calibration, and if multiple weights (cut pieces of copper wire) are used instead of a single piece that is moved along the length of the cantilever, the assumptions inherent herein can be avoided and a direct tip displacement vs tip force relationship attained.

4. FLOC MANIPULATION AND TESTING

This section describes the first attempts at floc manipulation. Larger holding pipettes and fine-tip manipulating pipettes were tried using, respectively, a coarse manual manipulator by Narishige and a fine electro-mechanical one (MP-285) by Sutter Instrument Co. Only one fine manipulator and only a very crude vacuum application assembly was available for testing at the Oakland University Biolab.

An example of using a larger diameter holding pipette is given in Fig. 34, where a floc was picked up and attached to a coarse holding pipette (~40 µm OD at the tip) using partial vacuum. The system used here did not have a way of applying a measured amount of suction. A simple device consisting of a small syringe attached to a micrometer was used. In this procedure, a micrometer was retracted a small distance and then the plunger of the syringe was manually followed, resulting in application of a small amount of suction, the results of which were visible under the microscope, as some fluid was seen entering the pipette. This fluid motion, when initiated close to the floc under consideration, pulled this floc with the fluid attaching the floc to the tip of the pipette and the floc stopping the flow. The suction then seemed to hold without any further application of additional suction throughout the short period of floc movement and manipulation (approximately 5 min). Under ideal conditions, the amount of suction can be controlled via a digital injector either initially, similar as here, or under a constant controlled application throughout an experiment. This controlled application may be beneficial for further numerical experiments to simulate the behavior of an individual floc as a more accurately descriptive boundary condition, where any vacuum loss is immediately restored by the system adjusting to any changes at the tip of the pipette. In our tests, vacuum application did not seem to damage the floc in any way and no visible change in surface geometry or internal floc features was observed. A drawback of this method was, however, that the amount of vacuum generated was not known quantitatively.

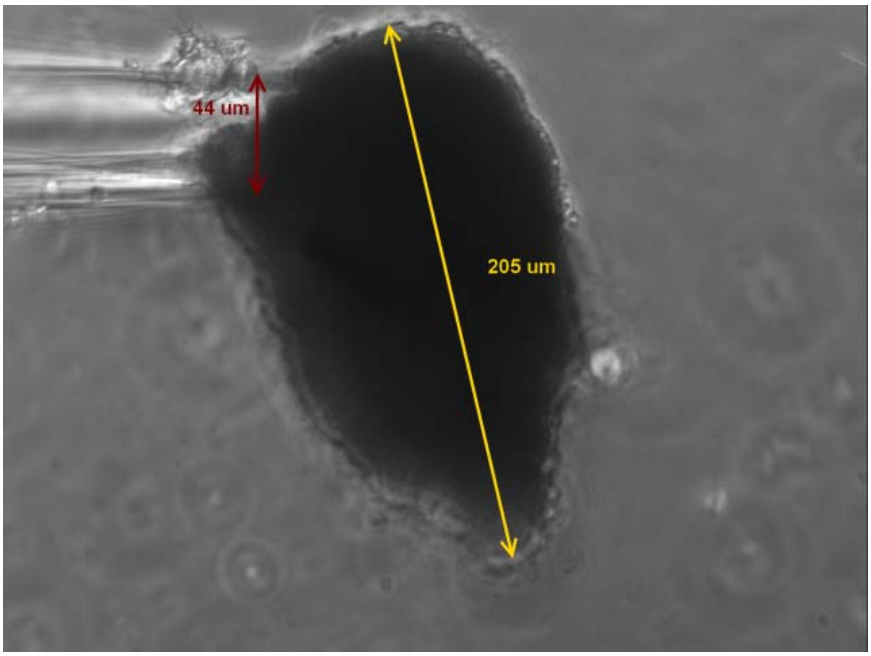

Fig. 34 – Holding pipette with the floc attached under partial vacuum (20X magnification, PLAN FLUOR objective, Sample 4 - 15 PSU salinity, 0% X-gum)

One of the concerns prior to this experiment was our ability to position a floc attached to a pipette in an area relatively free of any interstitial unaffiliated matter, found in abundance at certain combinations of the X-gum constituent and salinity of the liquid, as discussed above. During this experiment, we found that use of samples that contained a small amount of interstitial material simplified floc isolation, attachment to the tip of a micro-pipette, and subsequent relocation, when necessary, to a volume of liquid within the sample that is relatively free of small individual particles or other flocs. This means that testing of floc strength is possible without interference from other flocs, as can be seen in Fig. 34.

Overcoming surface tension during an insertion of the flexible (for force measurement) manipulated pipettes was an unexpected difficulty. Very small diameter and long cantilever pipettes are flexible enough that the surface tension generated by the fluid becomes a significant obstacle to the steady and measured advance of the tip of the pipette into the specimen. Often, the pipette will bend while the force is increased until the surface tension forces are overcome, after which, the pipette will move rapidly (and uncontrollably) down toward the bottom of the imaging chamber. This movement may be rapid and drastic enough to bend and even break off a tip of the micro-pipette in the process. A typical method of ameliorating the surface tension is to add a very small quantity of a Triton X-100 (a commonly used detergent in biological labs) surfactant. A small addition (e.g., 0.01 %) may be sufficient to attenuate the surface tension forces enough to allow for an easier insertion of the pipettes. In our planned experiments, larger diameter (hence, stiffer) micro-pipettes will be used; the increased pipette stiffness may in turn help overcome the surface tension.

In this preliminary investigation, after several attempts, the flexible pipette was inserted successfully and positioned near the floc. Application of the vacuum was not successful, however, as the small internal capillary was apparently closed. This was likely caused by suboptimal bending and micro-forging techniques used. Due to our inability to apply vacuum to both pipettes - the coarse holding one and the fine force-calibrated one - true testing of a floc's strength was no longer feasible. In the future tests, the procedure for bending the pipettes without interfering with the integrity of the pipette and maintaining the internal opening intact needs refinement. Sutter Instrument Company is advising that such techniques are indeed possible with proper selection of glass tubing with a more appropriate combination of inner and outer diameter, and with appropriate techniques of heating and bending the glass with a micro-forge.

Figure 35 shows an example of floc manipulation using two micro-pipettes – a coarse one of a patch-clamp style for static holding, and a flexible one for attachment, movements, and strength testing. Strength testing itself was not possible in this case, as was mentioned before, due to the inability to apply suction to this pipette. Figure 36 shows the same floc under higher magnification (20X, PLAN FLUOR) and after significant movements and manipulation. The floc was slightly reshaped as a result, with some dimension change, as indicated in the figure. Also shown are the dimensions of the tips of the two pipettes used, the patch-clamp holding pipette and the fine manipulating pipette.

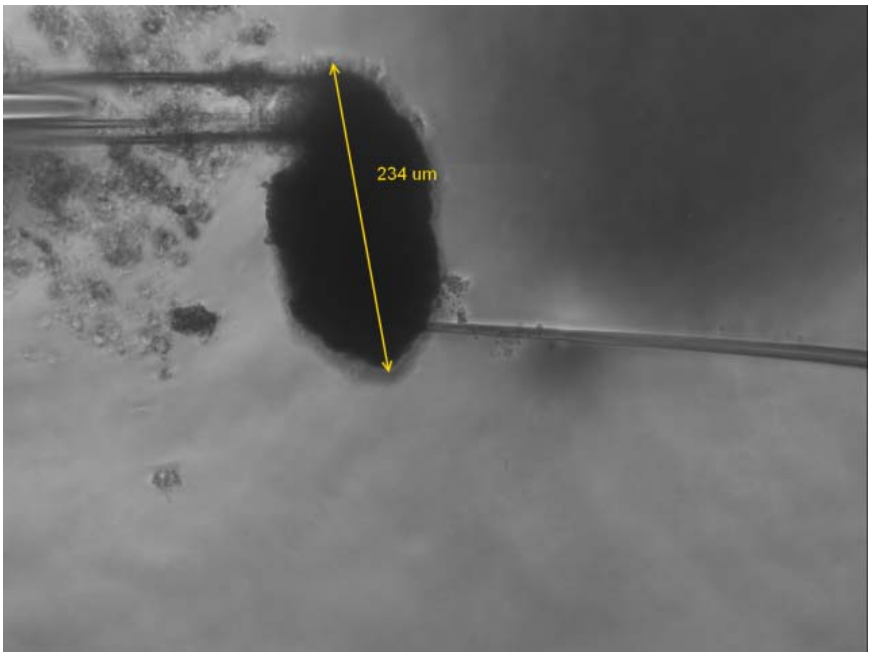

Fig. 35 – Manipulation of a floc (Sample 4: 15 PSU salinity, 0% X-gum) - coarse holding and fine manipulation pipettes (10X, PLAN FLUOR)

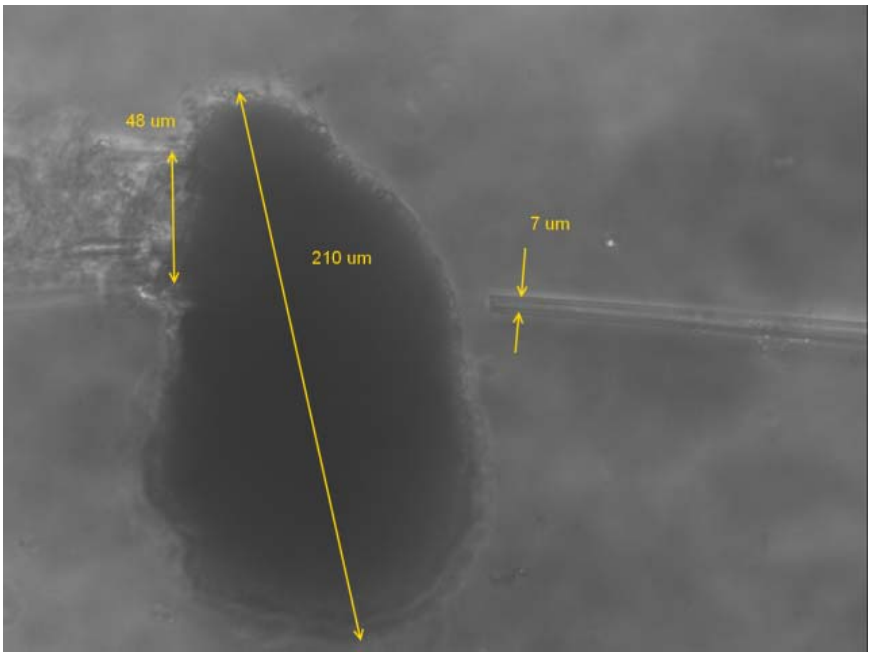

Fig. 36 – Manipulation of a floc (Sample 4: 15 PSU salinity, 0% X-gum) - coarse holding and fine manipulation pipettes, close-up (20X, PLAN FLUOR)

It is obvious that the fine pipette was much too small for strength testing, even if the application of vacuum had been successful. Thus the testing of the tensile strength would not have been realistic because the pipette, being too small compared with the floc, would have only detached small surficial elements of the floc, as opposed to the intended effect of splitting the floc into large parts, as was done in Yeung and Pelton (1996).

Manipulation of the floc with the two pipettes also yielded the following observation. Since the force-measuring pipette would have a longer and thinner cantilever, for more accurate force measurement, it would also undergo significant bending. This would make it impossible, or at least impractical, to have the entire thin cantilever in the microscope's field of view, as only very small magnifications would have to be used. Under these small magnifications, manipulation of flocs would be difficult to impossible to achieve. If the entire cantilever is not visible throughout the test, the deflection of the tip of this cantilever with respect to the movements of the base would not be measurable. If only the tip is visible, measuring this relative displacement can only be done if the position of the manipulator itself (i.e., the base of the micro-pipette) is monitored throughout the test and if the time sequence (as an output from the micro-manipulator's decoder) is synchronized with the time sequence available from the digital image processing, where the tip is visible and can be tracked. During the testing, proper attention should be given to this aspect of the problem to allow for the accurate measurements of the relative displacement of the flexible pipette's tip for high-resolution force measurement.

Alternatively, a different configuration of the manipulators can be used. One holding manipulator can be attached directly to the mechanical stage of the microscope, where any stage movements will not result in relative displacement of the stage-attached manipulator and the patch-clamp pipette holding the floc in place (relative to the imaging chamber). The second, fine (force-calibrated) manipulator can be attached to the table (fixed reference). In this case, when the suction is applied to the both pipettes in contact with the floc, instead of moving one of the manipulators (i.e., pipettes), the mechanical stage of the microscope (i.e., the imaging chamber) can itself be displaced, thus producing a displacement of the

specimen and equal displacement of the holding manipulator attached to the stage. The sample will move relative to the second manipulator, which is attached to the working table. In this case, digital imaging alone will be sufficient and no additional signal from the manipulator (electro-mechanical decoder) will be required to resolve the motion. Here, we will be able to measure (from the digital image analysis and particle tracking) the movements of the holding pipette with the sample, and the movements of the tip (or some other point close to the tip) of the flexible force-calibrated pipette. Thus, the requirement of placing the entire flexible cantilever within the field of view of the microscope will not be necessary. This method will also simplify the data acquisition system, as no additional electrical signals (from manipulator) will be needed and the entire measurement can be done solely based on the image processing.

5. CONCLUSIONS AND DISCUSSION

Several important conclusions have been drawn based on the results of this preliminary investigation into floc formation and manipulation, and pipette production and calibration, as well as the general hardware configuration to be used.

5.1 General Conclusions, Equipment, and Setup

In general, the optics selected for this test were appropriate and resulted in good ability to observe material via the eyepiece, as well as view and store the images digitally. The set of objectives used here included 10X and 20X PLAN FLUOR by Nikon that proved the most useful with the Phase Contrast illumination technique out of all those available for testing (Nikon T2000 microscope). These magnifications yielded a field of view appropriate for locating and manipulating flocs as well as capturing the images with the digital camera. The internal structure of the flocs was best viewed under the 40X magnification, for which another Nikon objective (PLAN APO) was used. The improved quality of the objective (higher numerical aperture values in APO vs FLUOR) allowed for good observation and image capture. Custom-made image chambers, used for these tests, proved very convenient as they possessed a glass (slip-cover #2) bottom cover allowing for good quality imaging using the Phase Contrast technique. The plexiglas cut-out slide, with the glass slip-cover attached to the bottom, proved easy to manipulate safely with the specimen in it and had small overall thickness (4 mm), convenient for pipette insertion and manipulation at shallow angles – an overall goal. This is necessary for floc testing (e.g., in tension) as it is the easiest to interpret the results of those tests where the forces are applied to a floc in the opposite directions along the same axis, thus producing pure tension conditions without additional torque or rotation generated. In our case, this would amount to attempting to apply these forces in the horizontal plane as much as possible. Other chambers or dishes with higher side walls would not be as effective in achieving this required condition.

Other equipment used included a Sutter Instrument Company pipette puller and mechanized micro-manipulator and a Narishige micro-forge. All of these devices were found appropriate for the different functions they performed and are also recommended for the NRL system along with a comparable Nikon microscope and objectives, as noted above.

5.2 Floc Formation as a Function of Salinity and Polysaccharide Content

The individual particles begin forming flocs at a minimum salinity of 5 PSU. Below that value (0 PSU tested only), the basic montmorillonite structures appear to be suspended in the liquid as individual particles of approximately 3 to 5 μm in size. This observation held true at the X-gum concentrations of 0 and 5% (of clay). At 10% X-gum, minimal flocculation was observed in a few small flocs. The majority of the matter was still relatively evenly dispersed throughout the suspension. Flocculation in general

occurred at all higher salinities tested (5 to 35 PSU), regardless of the presence or amount of the polysaccharide.

The full distribution of floc sizes was not studied systematically for each sample and only approximate conclusions can be drawn at this stage, based on a few select measurements. Every sample examined showed that the flocs appear in a variety of sizes for any one particular combination of X-gum content and salinity of the liquid. It appears that the size of the flocs increases with increasing salinity, including flocs in the smaller and larger size ranges – all increase in size at the higher salinity. Representative sizes measured show a gradual trend of size increase from around 30 μm in samples at 5 PSU to about 130 μm at 35 PSU. The largest flocs encountered for each suspension also increased proportionally, and occasionally, a very large "super-floc" would be found, exceeding the apparently average size by a factor of 3 or more.

The size distribution of the flocs appears to widen at the highest salinity examined (35 PSU). It appears that at this high salinity, the flocculation occurs fast enough and produces flocs of high density enough that the sedimentation to the bottom also accelerates. This trend may prevent some flocs from attaining their optimal (and larger) size under these conditions as they find their way to the bottom of the container with little interstitial basic components to continue to interact with. Thus, floc growth may be interrupted by sedimentation and packing on the bottom of the chamber, before maximum growth is achieved. This supposition requires further examination when more detailed data on floc size distribution becomes available.

Increase in the polysaccharide concentration also seems to increase the largest size of the floc encountered, but its effect on the average size is not apparent. It was noticed, however, that the increase in the X-gum content appeared to widen the size distribution of the flocs, at a particular salinity value. It was hypothesized that this effect could be due to the increase in the viscous forces in the liquid as a result of the higher polymeric content, resulting in delayed, and perhaps degraded, ability to flocculate. Further investigation and a systematic analysis are needed to draw definitive conclusions in this regard.

Additionally, samples at higher salinity showed apparent increase in the density of the internal structure of the flocs. Thus, at lower salinity (without noticeable dependence on polysaccharide concentration), the flocs appear to have more loosely attached appendages and the shape is much more irregular than at higher salinities, where the flocs appear much more rounded as spheroids or ellipsoids. This increase in floc density also influenced the apparent rate of sedimentation of the flocs to the bottom of the imaging chamber. In samples of higher salinity, rapid sedimentation seems to occur, with flocs forming a dense assembly with only small amount of interstitial space. Suspended flocs can still be found throughout the liquid, but these are fewer. The amount of interstitial matter in general decreases noticeably with increased salinity such that there is very little of it found at salinities above 20 PSU.

5.3 Pipette Drawing, Bending, and Calibrations

Pipette drawing was performed and was found to be easily accomplished. The factory recommended setting can be used as initial guesses for the pipette puller with further adjustments made as needed. Overall, pipettes with required diameters and long and relatively uniform cross-section cantilevers could be produced.

Pipette bending to produce L-shaped pipette tips, required for force-measurement, was not easily achieved, however. Best attempts resulted in tips bent to the appropriate angle but with the internal capillary closed. The internal capillary must remain open to allow vacuum application for floc attachment. More work in collaboration with pipette puller and forger manufacturers (Sutter Instrument Co., Narishige) is necessary to arrive at acceptable solutions here.

Pipette calibration was attempted using two different loading methods and utilizing a horizontally oriented microscope of the micro-forging device (Narishige). One involved electrostatic attachment of polystyrene beads and the other production and placement of small U-shaped pieces of wire as weights along the length of the pipette cantilever, oriented horizontally. The bead method has proven less reliable in our case of relatively larger forces and stiffer pipettes expected during the strength measurements of the flocs. The difficulty encountered was that the selected number of beads was not easily attached. The second method, however, proved superior and an example calibration was performed successfully using a single, U-shaped wire weight repositioned at a number of locations along the long cantilever. This method required relating forces imposed by this weight at different positions along the pipette to an equivalent force that, if applied at the tip, would produce the same tip deflection. This method requires some assumptions to be made regarding the flexural beam rigidity, which would not be necessary if multiple small weights, a third method, are used and all positioned near the cantilever tip. This third method is preferred and advised.

Floc manipulation was also performed successfully, where select flocs could be picked, isolated, and if needed, relocated to the volume of the liquid relatively free of additional interstitial matter, as would be important during actual strength testing. Since only one pipette (holding) was applying vacuum, no actual strength testing could be done. The second calibrated force pipette did not have an internal capillary open for vacuum application, and therefore, it was not possible to attach it to the other side of the floc. Preliminary indications are that the holding pipette can secure the floc and hold it throughout manipulation without interfering with its structure or eroding the surface of the floc. The actual amount of suction applied was not measured due to lack of proper equipment.

Overall, these initial trials may be considered successful in generating important knowledge about the flocs and their dependence on ingredients, pipette manufacturing and calibrations, and floc manipulation. Important conclusions regarding the equipment necessary for successful testing of flocs were made.

ACKNOWLEDGMENT

The author is thankful to Ms. Kathleen Lesich of the Oakland University's Biolab for sharing her experience in microscopy, micro-manipulators, and micro-pipette drawing and forging, as well as help in conducting the experiments described in this report. Thanks also are due to Dr. Charles Lindemann for allowing the use of the laboratory facilities and technical support personnel. My thanks also go to Drs. Y. Furukawa and P. Valent for the critical review and constructive comments on this report as well as to Drs. A. Reed and J. Dale (all of NRLSSC) for preparing the specimens.

REFERENCES

Schmitz, K.A., D. L. Holcomb-Wygle, D.J. Oberski, and C. Lindemann (2000). "Measurement of the force produced by an intact bull sperm flagellum in isometric arrest and estimation of the dynein stall force," *Biophys. J.* **79**(1), 468–478.

Timoshenko, S. (1940). *Strength of Materials. Part I: Elementary Theory and Problems* (D. Van Nostrant Publishing, Inc., New York).

Yeung, A. and R. Pelton (1996). "Micromechanics: A New Approach to Studying the Strength and Breakup of Flocs," *J. Colloid and Interface Science* **184**(2), 579-585.

Yoneda, M. (1960). "Force Exerted by a Single Cilium of Mytilus Edulis. I." *J. Experimental Biol.* **37**(3), 461-468.